DNA-DEPENDENT PROTEIN KINASE和其結合蛋白之生化及功能之研究(5/5)

成果報告

計畫編號：NSC 91 - 2321 - B002 - 004

執行期限：91/08/01 - 92/07/31

主持人：呂勝春 教授

執行機關：台灣大學醫學院分子醫學研究所

Nek9, a novel component of FACT-associated complex, modulates interphase progression

Bertrand Chin-Ming Tan[1] and Sheng-Chung Lee[1,2,3]*
Institutes of [1]Molecular Medicine and [2]Clinical Medicine,
College of Medicine, National Taiwan University, and
[3]Institute of Biological Chemistry, Academia Sinica,
Taipei, Taiwan

*Corresponding author
Mailing address:
Institute of Molecular Medicine
School of Medicine
National Taiwan University
7 Chung Shan South Road
Taipei, Taiwan
Telephone: 886-2-2356-2982
Fax: 886-2-2321-0977
E-mail: slee@ccms.ntu.edu.tw

Running title: Nek9 modulates interphase progression

Summary

The heterodimeric Spt16-Pob3/DUF/FACT complex is a class of chromatin structure modulator with important roles in replication and transcription. Although regarded as transcription elongator for chromatin template, little is known about mammalian FACT's mode of action and involvement in other molecular processes. Here, we report the identification of a novel interacting and functional partner of FACT, Nek9. Nek9 forms a stable, ~600 kDa complex with FACT in the interphase nuclei. Its active form is characterized by phosphorylation-dependent electrophoretic mobility shift and phosphorylation at a conserved residue within the activation loop (Thr_{210}). When complexed with FACT, Nek9 exhibits markedly elevated phosphorylation on Thr_{210}. Cell cycle analysis on the $Nek9^{dsRNAi}$ cells directly implicated Nek9 in maintaining proper G_1 and S progression, a role presumably related to the formation of a phospho-Nek9/FACT complex. Collectively, these observations provide evidence that Nek9, potentially as an active enzymatic partner of FACT, mediates certain FACT-associated cellular processes, which are ultimately essential for interphase progression.

Introduction

The human Spt16 and SSRP1 proteins constitute an abundant, nuclear, heterodimeric complex called FACT. FACT was initially discovered as chromatin-specific elongation factor that facilitate transcription of chromatin templates *in vitro* (1,2). The exact mechanism by which FACT aids the movement of RNA polymerase II along nucleosomal DNA is not known. However, FACT has been postulated to, through interacting with histone H2A/H2B dimers, render intranucleosomal histone connections more flexible (3).

The genes that encode these two FACT polypeptides, and more significantly, the existence of such stable heterodimeric factor, are highly conserved among eukaryotes. Homologous heterodimers have been purified and identified from yeast and frog cells. The *Xenopus* DUF (DNA unwinding factor) complex is also composed of Spt16 and SSRP1 homologs (4). Unlike the mammalian counterpart, DUF was directly implicated in DNA replication, as immunodepletion of this complex led to a reduced ability to replicate exogenously added sperm nuclei or plasmid DNA. However, its ability to alter nucleosomal DNA structure is conserved (5). Studies on the corresponding Spt16-Pob3 heterodimer in yeast have provided the most extensive evidence up-to-date on the pleiotropic nature of this heterodimer as well as its role as a chromatin structure modulator. Mutations in either genes cause various allele-specific defects in transcription initiation and elongation (6-8), and DNA replication (9,10). Additionally, conditional mutants exhibit stalled progression in G_1 and S

phases (10,11), perhaps as indirect consequences of misregulated chromatin processes. Consistently, genetic and physical interactions were observed between Spt16-Pob3 and a myriad of transcription or replication proteins, such as transcription elongator Paf1 complex (12,13), HAT complex NuA3 (14), histone deacetylase Rpd3 (9), general transcription factor TFIIE (15), putative chromatin factors San1 (16) and Chd1 (13,17), Nhp6 (a HMG protein that forms the SPN complex with the heterodimer) (9), DNA polymerase α (10,18), and various DNA replication factors (10,11,18). Collectively, this assortment of observations directly link FACT/DUF/Spt16-Pob3 to replication and transcription, and more specifically, to the structural regulation of chromatin, as such entity serves as template for both processes.

The existing evidence is consistent with the notion that FACT and homologous complexes possess a single central activity that is required for the progression of replication and transcription. However, their roles at multiple steps within these two processes may be mediated by differential coordination with various factors. The potential existence of such interaction network is substantiated by the aforementioned group of ySpt16-Pob3-interacting proteins. Hence, to further delineate human FACT's role in chromatin-related cellular processes, our research efforts have been focused on the identification and functional characterization of its interacting proteins. By generating monoclonal antibodies directed against SSRP1, and subsequently performing antibody affinity purification, we were able to isolate FACT-associated protein complexes from HeLa nuclear extracts. One of the

polypeptides identified in such search is the Nek9 protein.

Nek9 (previously termed Nek8) was originally identified as a β-casein kinase that associates with a putative substrate Bicd2 (19). It was independently identified as a Nek6- and Ran GTPase-binding protein under a different name, Nercc1 (20). Based on the kinase domain sequence similarity, Nek9 was a recent addition to the NIMA-like kinase (Nek) family, whose dozen or so members have diverse but relatively unknown functions. In addition to the N-terminal catalytic domain, Nek9 contains a central, RCC1-like, seven-repeats region, followed by a coiled-coil domain. Despite the presence of a NLS, previous publications have reported a cytoplasmic localization of this kinase. Furthermore, Nek9 is putatively involved in the microtubule dynamics and has been implicated in the regulation of mitotic progression (20).

Experimental results presented in this report confirm the presence of a nuclear form of Nek9. One of the major supporting evidence is the *in vivo* interaction between Nek9 and FACT, characterization of which was done using biochemical and immunocytochemical methods. A better mechanistic understanding of Nek9 was achieved by the discovery that, upon Nek9's autoactivation *in vitro*, the activation loop residue Thr_{210} was phosphorylated. We also demonstrated the novel existence of an endogenous phospho-Nek9/FACT complex, whose formation seems to rise during interphase. Interestingly, cells stably harboring the Nek9-targeting siRNA exhibited markedly slower progression of G_1 and S phases. Thus, our

data collectively suggest that Nek9, by virtue of forming an active kinase complex with FACT, may be involved in FACT-mediated functional pathways, compromise of which would ultimately lead to impeded interphase progression.

Experimental Procedures

Molecular cloning of the Nek9 cDNA

cDNA library was synthesized from poly(A)$^+$ RNA of HeLa cells. The complete open reading frame containing cDNAs were obtained from this library by PCR using LA *Tag* DNA polymerase (TaKaRa) with synthetic primers

5'-CCGCCATGTCGGTGCTGGGCGAGTACGA-3' (nek9-forward) and

5'-TGGGAACAGACTCCTGTAGACCCAGCCTC-3' (nek9-reverse, without the stop codon). The ~3 kbp fragment was subsequently subcloned into TOPO-TA plasmid (PCR II, Invitrogen) for sequence verification and further cloning. C-terminally FLAG-tagged Nek9 was produced by inserting a *NotI-SalI* fragment from the above Nek9-TA plasmid into the pCMV-Tag4A mammalian expression vector (Stratagene). C-terminal FLAG-tagged Nek9 was also subcloned into a baculovirus expression vector pVL1393 (PharMingen). For bacterial expression of recombinant Nek9, two partial coding sequences (*NotI-EcoRI* and *BamHI-EcoRI*, respectively corresponding to amino acids 1-266 and 291-559) were ligated to pET-32 prokaryotic expression plasmid (Novagen).

Preparation of recombinant proteins and antibodies

The expression plasmids pVL-Nek9-FLAG, pVL-Nek9-Myc, pVL-His_6-SSRP1, and pVL-FLAG-FACT140 were introduced into Sf9 insect cells using a BaculoGold transfection kit (PharMingen). The recombinant baculoviruses were produced and harvested according to the manufacturer's instructions. The Nek9-FLAG protein was purified by anti-FLAG (M2) immunoaffinity column and eluted with synthetic FLAG peptide (0.5 mg/ml). His-tagged Nek9s (amino acids 1-266 and 291-559), His-SSRP1, and His-FACT140 were expressed in BL21 (Lys) cells and purified from the clarified lysates on Ni-NTA agarose (Qiagen) according to the manufacturer's instructions. Monoclonal antibodies against SSRP1 (2B12, 3E4, 7F8, and 10D1) and FACT140 (8D2) were produced in mice using the respective recombinant proteins. Anti-Nek9 rabbit antisera, termed αNek9-N and αNek9-M were raised by independent injections with His-$Nek9_{1-266}$ and His-$Nek9_{291-559}$, respectively, and subsequently affinity purified through Nek9-FLAG column. Antisera against phosphorylated Nek9 activation loop peptide were generated in rabbits using KLH-conjugated phosphorylated peptides ($Nek9_{206-216}$: SMAET*LVGTPY, phosphorylated at Thr-210). The antisera from immunized rabbits were affinity purified successively with bacterial His-Nek9-conjugated and phosphorylated peptide columns. Both anti-Nek9 and Thr_{210}-Nek9 phospho-specific rabbit antibodies were produced by Dagene (Taiwan).

Immunoprecipitation, and western blot analysis

Cells were rinsed with PBS. Whole cell extracts were obtained using a buffer containing: 20 mM HEPES (pH 7.4), 0.2 M NaCl, 0.5% TX100, 5% glycerol, 1 mM EDTA, 1 mM EGTA, 10 mM β-glycerophosphate, 2 mM Na_3VO_4, 1 mM NaF, 1 mM DTT, plus protease inhibitors. Protein concentration was determined by the Bradford reagent (BioRad). Immunoprecipitations were done with the indicated antibodies prebound to protein G-Sepharose (Amersham), and washed in the cell lysis buffer containing 0.3 M NaCl. Similar conditions apply to the *in vitro* pull-down assay, in which lysates of Nek9-Myc were independently incubated with M2 (Sigma) and nickel (Ni-NTA, Qiagen) agarose beads pre-bound with FLAG-FACT140 and His_6-SSRP1, respectively. Western blot analysis was performed after electrophoretic separation of polypeptides by 7.5% or 10% SDS-PAGE and trasfer to Hybond-C membranes. Blots were probed with the indicated primary and appropriate secondary antibodies, and detected by ECL chemiluminescence (Amersham). Band signals on x-ray films were quantitatively analyzed by a Fujifilm Luminescent Image Analyzer LAS-1000plus and the software Image Gauge.

Gel-filtration fractionation

HeLa nuclei was isolated and lysed in nuclear extraction buffer (10 mM HEPES with pH 7.9,

10 mM KCl, 0.1 mM EDTA, 0.1 mM EGTA, 0.1% TX-100, 0.4 M NaCl, 10% glycerol and protease inhibitors). Nuclear extracts in the amount of 40 mg in a volume of 5 ml were loaded onto a precalibrated Sephacryl S-400 HR column with a bed volume of 135 ml (Pharmacia). Gel filtration was done in the same buffer at a flow rate of 0.5 ml/min. Ninety fractions were collected at 1.5-ml intervals. Upon fractionation, proteins present in each fraction were precipitated by adding 1/10 volumes of ice-cold 100% TCA. Recovered samples were run on SDS-PAGE and analyzed by Western blotting using the indicated antibodies. For detection of FACT-associated complexes, immunoprecipitation was carried out with 10D1 on equal amounts of the selected fractions. Precipitated polypeptides were electrophoretically separated and analyzed by Western blotting.

Indirect immunofluorescence and confocal microscopy

All steps of the immunostaining procedure were done at room temperature. HeLa cells were first washed with PBS twice followed by fixation with fresh 2% paraformaldehyde in PBS for 15 minutes. After brief rinse in PBS, cells were permeabilized with 0.5% Triton X-100 in PBS, blocked with 1% BSA in PBS, and probed with the indicated primary antibodies. Secondary antibody incubation was done for 1 h using Alexa 488 conjugated goat anti-rabbit IgG and Alexa Fluor 594 conjugated goat anti-mouse IgG (Moleular Probes, Inc). To visualize DNA, cells were counter-stained with DAPI. For detection of DNA replication sites, HeLa cells on

coverslips were pulse labeled with 10 μM BrdU at 37℃ for 30 min. Upon fixation and permeabilization, cells were subjected sequentially to acid treatment and trypsin enzymetic digestion before being stained (mouse anti-BrdU, Sigma). Stained cells were analyzed with the Zeiss LSM-510 inverted confocal laser-scanning microscope, using a 63X/NA 1.4 oil immersion objective lens.

Cell culture, transfection, and cell cycle synchronization

All HeLa cells were maintained in Dulbecco's modified Eagle's medium supplemented with 10% fetal bovine serum and 100 units/ml penicillin and streptomycin. Cells were transfected using Lipofectamine (GIBCO) according to the manufacturer's instructions. To establish a plasmid-based dsRNAi system targeting endogenous Nek9, annealed oligonucleotides corresponding to partial Nek9 sequence were designed and ligated to the p*Silencer* 1.0-U6 vector (Ambion) according to the manufacturer's instructions. The cDNA sequence of the targeted Nek9 mRNA region is: 5'-GACCATCCGTTCCAATAGC-3' (nucleotides 2193-2211). The same sequence in the inverted orientation was used as the non-specific dsRNAi control. Generation of cell lines stably harboring dsRNAi was done by first co-transfecting HeLa cells with pcDNA3 plasmid (bearing Neomycin selection gene) and the ligated p*Silencer* 1.0-U6 vectors. Positive clones were selected subsequent to a 14-day culturing in the presence of 1 mg/ml G418, and eventually maintained with 0.2 mg/ml G418.

For M phase synchronization, subconfluent cells were treated with 200 ng/ml nocodazole for 10 hours. Mitotic cells were harvested through detachment by mitotic shake-off. Cells remained on the flasks after shake-off were harvested by trypsionization and regarded as G_2 cells. Cells were synchronized at the G_1/S boundary by double thymidine block. Subconfluent culture was blocked with 2 mM thymidine (final) and incubated for 19 hours. Cells were washed three times with PBS, and then incubated with fresh serum-rich medium for 10 hours. Subsequently, the second block with 2 mM thymidine lasted for 15 hours, after which the cells were released by extensive washes with PBS. For determination of active DNA replication, immediately before harvest at each time point, cells were pulse-labeled with 10 μM BrdUTP for 15 mins. After harvest by trypsinization, cells were fixed with ethanol (70% final), denatured in 2N HCl for 30 min at 37℃, and subsequently enzymetically treated with trypsin for 30 min at 37℃. Cell cycle profiles and degree of BrdU labeling were monitored by FACS.

Colony formation assay

Different clones of both the wild-type and $Nek9^{RNAi}$ cells were seeded into 6-cm diameter tissue culture dishes at 600 or 1200 cells per dish, in triplicate, and grown in the presence of 100 μg/ml G418. Dishes were incubated for 10-12 days in a humidified incubator at 37℃. Colonies were subsequently fixed with methanol and stained with 1% crystal violet.

Fluorescence-activated cell sorting (FACS) analysis

Control and Nek9^{RNAi} cells, after being released from the double thymidine block or mitotic shake-off, were collected by trypsinization at the indicated time points. Cells were washed and then fixed with 70% ethanol for $\geqq$ 2 h on ice. Cells were stained with DNA staining solution (100μg/ml propidium iodine, 100μg/ml RNase A, and 0.5% NP-40 in PBS) at room temperature for 30 min. DNA content was analyzed, based on emissions recorded in the FL-2 channel, from 10,000 cells (events) within the fluorescence gate, using a Beckton Dickinson Flow Cytometer in conjunction with the CellQuest software. To detect cells actively undergoing DNA replication, BrdU incorporation was identified using anti-BrdU mAb, followed by Alexa 488-conjugated secondary antibodies, with emissions recorded in the FL-1 channel. The labeling index is determined by calculating the ratio of the gated BrdU-positive cells relative to the total events.

Immunocomplex kinase assay

Whole cell extracts were subjected to immunoprecipitation as described above with the indicated antibodies. Immunocomplexes were washed extensive with lysis buffer (0.3 M NaCl) and equilibrated with the kinase buffer (50 mM Tris at pH 7.4, 5 mM $MgCl_2$, 5 mM $MnCl_2$, and 1 mM DTT). For autoactivation, immobilized Nek9 or associated complexes were

incubated in kinase buffer supplemented with 100 μM ATP at 25℃ for 20 min. Activation was stopped by either adding electrophoresis sample buffer, where appropriate, or by washing the beads in kinase buffer. Subsequently, activity was assayed by incubation at 30℃ in kinase buffer plus 5 μM ATP, 100 μCi/ml [γ-32P]ATP (Amersham), and 1 μg of histone H1. Reactions were terminated by adding 4X Laemmli SDS sample buffer and boiling. Denatured samples were resolved by SDS-PAGE.

Peptide identification by mass spectrometry and bioinformatics analysis

The gel piece containing selected polypeptides was first reduced and pyridylethylated as described previously (21). Up to 0.2 μg of the enzyme trypsin (Promega) was added to the dried gel. After overnight incubation, the supernatant was removed and the gel was extracted twice with adequate amount of 0.1% formic acid. The supernatant and the extracts were combined together and dried in a Speed-Vac, and re-suspended in 0.1% formic acid immediately before use. Electrospray mass spectrometry was performed using a Finnigan Mat LCQ ion trap mass spectrometer interfaced with an ABI 140D HPLC (Perkin-Elmer). A 150 x 0.5 mm PE Brownlee C18 column (Perkin-Elmer) (5 mm particle diameter, 300 Å pore size) with mobile phases of A (0.1% formic acid in water) and B (0.085% formic acid in acetonitrile) were used. The peptides were eluted using the acetonitrile gradient and analyzed by "triple-play" experiment as described (21). Data interpretation as well as correlation

between the spectra and amino acid sequences within a human EST database was done by a Finnigan Corporation software package, the SEQUEST Browser.

Homology searches were carried out with BLAST (22) and PSI-BLAST (23) against the PDB (Protein Data Bank). The Nek9 kinase domain and the structure-solved homologues were aligned with BCM Search Launcher (24). Alignment manipulations were carried out with Jalview (http://www.ebi.ac.uk/~michele/jalview/) and ESPRIPT (25).

Models were built with MODELLER-6 (26) starting from the alignments shown in Figure 3A. Models derived from initial alignments were subjected to packing analysis with PROSA II (27) and stereochemical analysis with PROCHECK. Regions of atypical packing (positive stretches in the resulting PROSA II profiles) or stereochemical problems were subjected to alignment adjustments and new models made. The adjustments were either alignment shifts or changes in the template(s) used for a particular region. Alignment adjustments resulting in improved models were accepted and new improvements sought until no more could be obtained. Finally, 10 structures were generated, and the one with the best objective function was kept.

Results

Identification of Nek9 as a novel associated protein of FACT

To identify the key binding partner for the hSpt16-SSRP1 complex, we undertook the

immunoaffinity purification scheme to isolate SSRP1-containing protein complexes from the cell nuclei. Nuclear extracts were subjected to immunoprecipitation with anti-SSRP1 monoclonal antibodies (clone 10D1). As shown in Figure 1A, the major protein bands of 140 kDa and 90 kDa correspond to hSpt16 and SSRP1, respectively, as confirmed by Western blot and mass spectrometric analyses (data not shown). Such affinity purification also recovers a 120 kDa polypeptide with approximate stoichiometry to FACT. Subsequent spectrometric analysis of this band revealed a sequence match of the identified spectra to the coding sequence of the human Nek9 protein. To further characterize this protein, we generated and affinity-purified polyclonal antibodies against different parts of Nek9, termed αNek9-M (spanning amino acids 291-559) and αNek9-N (1-291). Both antibodies specifically recognize a 120-kDa polypeptide in the HeLa cell extracts as well as in the monoclonal antibody 10D1-targeted immunocomplex (Figure 1B and data not shown). Other anti-SSRP1 monoclonal antibodies, whose approximate epitotpe regions have been mapped using deletion constructs of SSRP1 (Figure 1B, lower panel), were subjected to immunoprecipitation experiments as well. Nek9 was also detected in the immunoprecipitates pulled down by 7F8, but not in those targeted by 3E4 and 2B12, thus indicating its specific association with distinct FACT complexes (Figure 1B). Additionally, because 10D1 and 7F8 did not cross-react towards Nek9 immunochemically (Figures 1B, 1F, and data not shown), we excluded the possibility here that the co-immunoprecipitated Nek9 arose from non-specific

antibody-epitope binding. While performing a reciprocal co-immunoprecipitation experiment using the anti-Nek9 antibodies, we were able to identify FACT heterodimers in the αNek9-N immunocomplex (Figure 1C). Immunoprecipitates targeted by αNek9-M, on the other hand, did not contain FACT (Figure 4A and data not shown). Such observation suggests that there is a fraction of Nek9 that is free of FACT in the cells. Altogether, these immunoprecipitation results demonstrate the unique presence of a FACT/Nek9 protein complex *in vivo*.

Nek9 interacts with FACT to form a ~600-kDa complex

To unequivocally delineate the specific interaction between Nek9 and FACT, we carried out an *in vitro* pull-down assay using baculovirus-derived recombinant proteins (Figure 1D). Myc-tagged Nek9 was found to bind immobilized FLAG-FACT140 (lane 2) and His_6-SSRP1 (lane 4), whereas no interaction between Myc-Nek9 and other similarly tagged proteins was observed (lanes 5 and 6). Interaction of Nek9 with SSRP1 was also verified through co-infection of respective recombinant baculoviruses followed by co-immunoprecipitation analyses using the M2 antibody (Figure 1E).

Next, in a gel-filtration chromatography (using Sephacryl S-400) of the HeLa nuclear extracts, Nek9 elutes with a molecular mass of ~600 kDa, which is consistent with previous observation (20) (Figure 1F). FACT has overlapping but broader distributions in fractions and appears to exist in higher molecular size protein complexes. To further establish the coelution

of the FACT and Nek9 polypeptides, antibody 10D1 was used to carry out immunoprecipitation on selected fractions. Nek9 was found in the FACT-containing complexes isolated from fractions #20-28, coinciding with the elution profile of endogenous Nek9. Similar coelution profile was also observed with the 7F8 antibody (data not shown). Taken together, these results validate the stable association of Nek9 with a distinct FACT complex *in vivo*, whose size is around 600 kDa. However, we cannot presently rule out the possibility of the presence of additional factors in the FACT-Nek9 complexes due to the larger-than-expected molecular mass for the heterotrimer.

Nek9 and FACT colocalize in the interphase nucleus, are similarly free from condensed chromatin, but dissociate from each other during chromatin decondensation

The subcellular localization of the endogenous Nek9 protein was determined by indirect immunofluorescence using the polyclonal antisera directed against Nek9. Results of confocal microscopic analysis indicate that, consistent with the above biochemical evidence, Nek9 exhibits a nuclear distribution in HeLa cells (Figure 2A, a and b). On the other hand, although ectopically expressed FLAG-Nek9 distributed predominantly in the nucleus (Figure 2B, a), we also observed nucleocytoplasmic and cytoplasmic staining in some cells (Figure 2B, b). To better characterize the nature of the endogenous FACT-Nek9 association, co-localization experiments were performed simultaneously. In the interphase nuclei, we detected a

discernible degree of overlap in staining patterns between Nek9 and either component of the FACT complex (Figure 2A, a and b). On the other hand, the presence of non-merged signals concurs with the above observation that a fraction of the endogenous Nek9 does not associate with FACT, and vice versa. In cells that enter mitosis, the immunoreactive signals of Nek9, FACT140, and SSRP1 become similarly diffused and entirely excluded from the condensed chromatin (Figure 2A, c-f; data not shown for FACT140). Interestingly, a significant disjunction of anti-Nek9 and anti-FACT staining patterns was observed in post-cytokinetic cells (Figure 2A, g). FACT seems to reassociate with decondensing chromatin at this point, whereas Nek9 remains diffused and free from chromatin. However, in post-cytokinetic cells with less aggregated DAPI-staining, representative of nucleus establishment and interphase initiation, the localizations of Nek9 and FACT can be seen partially merged again (Figure 2A, h). Together, these data demonstrate that the subcellular locations of Nek9, as well as FACT, alter throughout the cell cycle.

The Thr_{210} residue locates within the activation loop region of Nek9 and is conserved among various kinases

Toward a better mechanistic understanding of the catalytic attributes of Nek9, we performed bioinformatic analysis. Among Nek family proteins, there is extensive sequence conservation within the kinase domain. In comparison with other unrelated kinase proteins,

residues critical for catalysis and structural folding are also preserved in Nek9 (Figure 3A). Using existing structural information of selected kinases as templates, 3-dimensional comparative model of the Nek9 kinase domain has been generated (Figure 3B). The putative active site is surrounded and formed by the characteristic β-sheets and helix bundle, with the activation loop located outside the catalytic pocket. Previous study using the peptide substrate demonstrated that Nek9 was able to phosphorylate *in vitro* the Thr_{210} residue within the activation loop region, thus indicating Nek9's potential ability to autophosphorylate (19). Based on the sequence comparison, Nek family members are fairly conserved at this residue as well as in the surrounding region (Figure 3C). From a structural standpoint, the Thr_{210} residue is situated at a rather exposed area that is accessible to modification (Figure 3B).

Upon autoactivation, Nek9 undergoes phosphorylation-dependent electrophoretic mobility shift and phosphorylation on Thr_{210}

To assess whether phosphorylation indeed occurs on Thr_{210} as well as the relationship between such phosphorylation and the kinase activity, we generated polyclonal antibodies that specifically recognize phsophorylated Thr_{210} of Nek9. Similar to the previously reported results on transfected FLAG-Nek9, endogenous, immunoprecipitated Nek9 kinase became activated (i.e. phosphorylation on histone H1) upon pre-incubation with a high concentration of ATP (100 μM) (Figure 3D, lane 3). Interestingly, we observed that the majority of Nek9

underwent electrophoretic mobility shift only at the high ATP concentration. Phosphorylation on Thr_{210} accompanies this decrease in mobility, as such slower-moving form was detectable using the phospho-specific antibody. The specificity of this antibody was revealed by the lack of immunoreactive signals from the non-shifted species of Nek9 (Figure 3D, lanes 1 and 2). This observation also suggests that phosphorylation at Thr_{210} was absent or at very low level on the non-activated Nek9 polypeptides. Note that the immunoprecipitates possessed minimal activity when pre-incubated with no or low ATP, implying a likely requirement of endogenous Nek9 and its autoactivation for the optimal H1 kinase activity. The 10D1-targeted FACT-complexed Nek9 had similar enzymatic behaviors upon kinase activation (data not shown).

The ATP-induced electrophoretic retardation of Nek9 can be attributed to addition of the phosphate moiety, due to the fact that treatment with alkaline phosphatase following kinase autoactivation abolished such positional shift on the gel (Figure 3E, lanes 1-3). Consistently, the accompanying immunoreactivity toward the Thr_{210} phospho-specific antibody was also found directly linked to phosphorylation. Previous reports have demonstrated that the mitotic form of Nek9 has a retarded electrophoretic mobility. To address the issue of whether the mitotic and the autoactivated, Thr_{210}-phosphorylated form of Nek9 share similar characteristics, we performed immunoblotting on Nek9 isolated from different cell cycle phases. We could routinely observe differences in mobility among the *in vitro*

autophosphorylated Nek9, mitotic Nek9, and Nek9 isolated from asynchronous culture (Figure 3E, lanes 4-6). Furthermore, the mitotic Nek9 is not phosphorylated at the Thr_{210} residue (data not shown), additionally implying that these two forms of Nek9 may represent distinct species.

Phospho-Nek9 associates with FACT in a cell cycle-dependent manner

Next, to examine the possibility that the up-shifted, Thr_{210}-phosphorylated form of Nek9 is an endogenous entity, we probed for its presence in the cell extracts. Using the phospho-specific antibody, we were able to detect a protein band with the mobility and immunoreactivity characteristic of the activated form of Nek9 (Figure 4A, lane 1). In addition, this antibody also recognized a band, whose existence was phosphatase-sensitive (data not shown), in the 10D1-targeted (Figure 4A, lane 3) and the 7F8-targed (data not shown) immunocomplexes. Conversely, no phosphorylated form was found present in the αNek9-M-immunoprecipitates, which are free of FACT (lane 5). These results strongly support the existence of an active, phsophorylated form of Nek9 as well as a phospho-Nek9/FACT complex *in vivo*. This specific and preferential association of the phosphorylated form of Nek9 with the FACT complex indicates that, in the presence of FACT, Nek9 may undergo a marked elevation in Thr_{210}-phosphorylation.

In an attempt to further characterize the nature of the phospho-Nek9/FACT complex, we

next inspected whether the level of Thr_{210}-phosphorylation on FACT-bound Nek9 is regulated in a cell cycle-dependent manner. FACT complexes at different stages of the cell cycle were immunoprecipitated and subsequently probed for the Thr_{210}-phosphorylated Nek9. As shown in Figure 4B, there is a constitutive presence of phospho-Nek9 in the FACT immunocomplexes throughout different phases. However, the levels of association seemed to rise upon release from the G_1/S phase block (lanes 1-4), and undergo detectable reduction in the M and G_2 phases (compare lanes 5 and 6). Such observed variation potentially reflects an interphase-specific elevation in the formation of the active, phospho-Nek9/FACT complex.

RNAi-mediated knock-down of Nek9 proteins triggers interphase delay

Next, toward elucidating the cellular roles of Nek9 and further examining its link to interphase, we undertook a vector-based siRNA approach to abrogate endogenous Nek9 expression in HeLa cells. Successful establishment of independent clones stably harboring Nek9-interfering dsRNA was confirmed by Western analysis on cell lysate proteins, as shown in Figure 5A. While the level of control protein remained the same, <30% of the endogenous Nek9 polypeptides were detected in the two $Nek9^{RNAi}$ clones as compared to the control clones.

While maintaining the culture of these stable clones, we unexpectedly observed relatively slower growth of the $Nek9^{RNAi}$ cells. To examine this phenotype more closely, we

performed colony formation assay. Independent experiments have demonstrated that, after two-week culturing, $Nek9^{RNAi}$ cells yielded dramatically smaller colonies than the control cells, clearly a consequence of a stalled cell growth (Figure 5B). To further explore the possible underlying attributes of such retarded proliferation, these stable cells were subjected to synchronization studies. First, cells were synchronized through nocodazole-mitotic shake-off treatment. At different time points, cells were collected and DNA content was determined by FACS analysis. As shown in Figure 6A, the rates of appearance for cells with a DNA content of 2N (representative of G_1 phase) were unchanged regardless of the levels of Nek9 proteins. However, the $Nek9^{RNAi}$ cells seemed to move through the G_1 phase at a slower pace and consequently initiate S phase approximately 3-4 hours later than control cells.

In a separate experiment, double thymidine block was used to monitor cell cycle progression through the G_1/S point. Results depicted in Figure 6B evidently indicate a delayed S phase in the $Nek9^{RNAi}$ culture. On the other hand, the progression of G_2/M phase appeared normal in this cell line, comparable to the above nocodazole experiment. Similar experiment was also carried out to quantitatively assess the population of actively replicating cells at different times upon removal of the block. Cells were pulse-labeled with BrdUTP before being harvested at the designated time points. The ratio of the BrdU-positive cells, termed the "labeling index", represents the population of cells that actively synthesize DNA in a particular culture. By plotting the changes in the labeling indexes in relation to time, a similar

trend was observed in which the Nek9^{RNAi} cells exhibited markedly delayed S phase, specifically at the onset stage (Figure 6C). Collectively, data from the RNAi experiments indicates that adequate level of Nek9 is essential for G_1/S transition and S phase progression.

Discussion

In the present study, we identified Nek9 as a novel component of the FACT-associated multiprotein complexes, and performed functional characterization of this protein. Their *in vivo* interaction was demonstrated using biochemical as well as cell biological methods. Most notably, a considerable portion of the endogenous Nek9 polypeptides are stably bound to FACT, although gel-filtration and immunoprecipitation analyses indicated that the FACT-Nek9 complex represents only a fraction of the total FACT-associated complexes population. It is interesting to note that the only presently known human FACT-interacting proteins are both kinases. Besides Nek9, CK2 was recently found to form an UV-induced, p53-targeting complex with FACT (28,29). Although both complexes differ physically and functionally, their existence consistently implicates FACT in the progression of cell cycle (i.e. interphase), and further supports a potential role of post-translational modification (i.e. phosphorylation) in FACT-associated processes.

Despite the presence of an NLS in Nek9, previous reports have demonstrated a cytoplasmic localization of this protein as well as its putative roles related to its subcellular

location (i.e. regulation of microtubule dynamics and mitosis) (19,20). In this report, we have provided several lines of experimental evidence supporting the existence of a nuclear counterpart of the human Nek9 protein: 1) the immunochemical detection of Nek9 in the nuclear extract preparation; 2) the biochemical demonstration of the stable association of a large pool of Nek9 polypeptides with the FACT heterodimers, which are primarily nuclear factors; and 3) the immunocytochemical characterization of Nek9's nuclear localization and association with euchromatin (acetyl-histone H3) regions (data not shown).

Our results uncovered a novel functional aspect of Nek9 that is different from previous reports: the involvement in the progression of interphase. Using Nek9-specific antibody microinjection in prophase cells, Roig *et al.* have observed spindle and chromosome abnormalities characteristic of misregulated mitosis (20). However, when antibodies were injected in interphase cells, they failed to enter mitosis, indicative of stalled cell cycle progression. Such preliminary observation is in agreement with the behaviors of our $Nek9^{RNAi}$ cells, and further pinpointing an equally important role of Nek9 in the interphase. On the other hand, based on our synchronization/DNA content analysis on the knock-down cell line, no delay or abnormal progression of mitosis was detected. It is possible that Nek9's mitotic activity would not be compromised unless the protein levels are further diminished below a critical threshold, or other unknown post-translational regulation is interfered. Interestingly, results obtained from our cell cycle analysis of the $Nek9^{RNAi}$ cells bear close resemblance to

previous mutant phenotypic studies in the yeast *Saccharomyces cerevisiae*. *CDC68*, the yeast counterpart of the human Spt16 gene, was found in a screen for genes required for Start, and consistently, cells with mutation in this gene (*cdc68-1*) were conditionally arrested in the G_1 stage (10). In an independent study, mutation in *POB3*, the homologue of SSRP1, was found to cause delay in S phase onset and progression (11). Correlation among these cell cycle-related mutant phenotypes directly strengthens the physiological relevance of the FACT-Nek9 interaction. Furthermore, the observed role in interphase may be temporally related to an increase in Thr_{210}-phosphorylation on the FACT-bound Nek9 (Figure 4B). Based on these results, we postulate that Nek9, in association with FACT, may be actively involved in certain important FACT-related functions, compromise of which would ultimately lead to impeded interphase progression.

Results of the colocalization experiments revealed an interesting feature of the formation of the endogenous FACT-Nek9 complexes: although normally existing as an otherwise stable complex, FACT-Nek9 briefly separates at the M-G_1 transition. We performed additional immunoprecipitation experiments with lysates derived from cells arrested at different cell cycle phases and found no differences in the co-immunocomplex profiles as compared to that of the asynchronous culture (Figure 4B and data not shown). However, it may be difficult to detect such absence of complex association due to its transient nature as well as depending on the lysate extraction condition. Nevertheless, our observation of the divergent localization

between FACT and Nek9 at the end of mitotis signals a physical, and possibly functional, separation of the FACT-Nek9 complex at this particular stage. It is also possible that the formation of such protein complex has a temporal dependence on the establishment of nuclear envelope and appropriate chromatin state. Furthermore, the novel observation of the cyclic manner in which FACT becomes excluded from condensed chromatin and then reassociates with decondensing one is consistent with FACT's putative mode of action: facilitating the accessibility of chromatin. Such regulated movement can prevent any untimely loosening of the condensed chromosomes, which is catastrophic to the mitotic progression.

Our results on the mechanistic characterization of Nek9 provide another example of enzymatic autoactivation. Although it is currently unclear why the higher-than-physiological concentration of ATP is required for activation, some of the above characteristics are reminiscent of some other kinases such as Aurora A kinase and Polo-like kinase Plk-1 (30-32). Consistent with the previous observations, our results based on the use of the anti-phospho-Thr_{210} antibody have demonstrated an important role of the activation loop structure in the upregulation of kinase. Based on the hypothetical structural model, it is probable that phosphorylation at the threonine location may lead to negative charge-mediated structural changes (i.e. catalytic pocket opening), which ultimately are more favorable for substrate targeting.

Most notably, utilizing the phospho-specific antibody, we have achieved the novel

finding on the existence of the lower-mobility, Thr_{210}-phosphorylated species of Nek9 *in vivo*. Due to the extensive kinase domain conservation among the Nek family members, it is possible that Nek9's catalytic attributes *in vitro* and *in vivo* are widely shared by others. The presence of the phosphorylated Nek9 in the FACT-associated immunocomplex indicates that a fraction of the complexed Nek9 remains in a steady-state active form. The finding of the preferential association of phospho-Nek9 with FACT *in vivo* provides evidence that interacting with FACT may render the kinase more active. The possibility of FACT acting as a non-kinase activator of Nek9 as well as the exact mechanism through which FACT alters Nek9's catalytic property await further study.

The complex and multiple roles of FACT heterodimer in DNA replication, transcription initiation, and transcription elongation are well established through various genetic and biochemical studies done on different homologs. Based on the results obtained from the yeast system, Formosa *et al.* postulated that this heterodimer has a single central activity of altering the chromatin, while its roles at different stages of replication and transcription might be mediated through coordinately functioning with other factors (9). This interaction network has been experimentally established by the discovery of various genetic and physical interactors of FACT. It is interesting to note that, upon gel filtration on crude extract materials (Figure 1F), the peak fractions of FACT were in a range that is much higher than the expected native mass of purified FACT, which is about 230 kDa (1). Such faster and broad elution profile of

FACT provides another strong evidence for the existence of different multiprotein complexes. Surprisingly, in the immunoprecipitates of some of the fractions, our FACT-specific antibodies could detect additional protein bands that had different electrophoretic mobilities (Figure 1F). This raises the possibility that, on top of protein interaction, post-translational modifications may also be present and of some significance in the regulation of FACT activities. Finally, the addition of Nek9 to the growing list of FACT-interacting factors may either suggest a novel pathway of this FACT complex, or indicate the involvement of phosphorylation-dependent signal transduction in the existing FACT-associated processes. Thus, identification of physiological substrates targeted by the kinase complex may be of great importance in its functional characterization.

Acknowledgements

We are grateful for the modeling and bioinformatic work performed by Dr. Chun-Hua Hsu. We especially thank Dr. Stephen J. Lippard for generously providing the SSRP1 expression vector, Drs. Danny Reinberg and Ruey-Hwa Chen for critical discussions, and Dr.Yeou-Guang Tsay for assistance with mass spectrometric analysis.

This research was supported by grants from National Science Council (NSC90-2321-B002-003) and the Institute of Biological Chemistry, Academia Sinica, Taiwan.

References

1. Orphanides, G., LeRoy, G., Chang, C. H., Luse, D. S., and Reinberg, D. (1998) *Cell* **92**, 105-116.
2. LeRoy, G., Orphanides, G., Lane, W. S., and Reinberg, D. (1998) *Science* **282**, 1900-1904.
3. Orphanides, G., Wu, W. H., Lane, W. S., Hampsey, M., and Reinberg, D. (1999) *Nature* **400**, 284-288.
4. Okuhara, K., Ohta, K., Seo, H., Shioda, M., Yamada, T., Tanaka, Y., Dohmae, N., Seyama, Y., Shibata, T., and Murofushi, H. (1999) *Curr Biol* **9**, 341-350.
5. Seo, H., Okuhara, K., Kurumizaka, H., Yamada, T., Shibata, T., Ohta, K., Akiyama, T., and Murofushi, H. (2003) *Biochem Biophys Res Commun* **303**, 8-13.
6. Brewster, N. K., Johnston, G. C., and Singer, R. A. (2001) *Mol Cell Biol* **21**, 3491-3502.
7. Evans, D. R., Brewster, N. K., Xu, Q., Rowley, A., Altheim, B. A., Johnston, G. C., and Singer, R. A. (1998) *Genetics* **150**, 1393-1405.
8. Formosa, T., Ruone, S., Adams, M. D., Olsen, A. E., Eriksson, P., Yu, Y., Rhoades, A. R., Kaufman, P. D., and Stillman, D. J. (2002) *Genetics* **162**, 1557-1571.
9. Formosa, T., Eriksson, P., Wittmeyer, J., Ginn, J., Yu, Y., and Stillman, D. J. (2001) *Embo J* **20**, 3506-3517.
10. Wittmeyer, J., and Formosa, T. (1997) *Mol Cell Biol* **17**, 4178-4190.
11. Schlesinger, M. B., and Formosa, T. (2000) *Genetics* **155**, 1593-1606.
12. Squazzo, S. L., Costa, P. J., Lindstrom, D. L., Kumer, K. E., Simic, R., Jennings, J. L., Link, A. J., Arndt, K. M., and Hartzog, G. A. (2002) *Embo J* **21**, 1764-1774.
13. Krogan, N. J., Kim, M., Ahn, S. H., Zhong, G., Kobor, M. S., Cagney, G., Emili, A., Shilatifard, A., Buratowski, S., and Greenblatt, J. F. (2002) *Mol Cell Biol* **22**, 6979-6992.
14. John, S., Howe, L., Tafrov, S. T., Grant, P. A., Sternglanz, R., and Workman, J. L. (2000) *Genes Dev* **14**, 1196-1208.
15. Kang, S. W., Kuzuhara, T., and Horikoshi, M. (2000) *Genes Cells* **5**, 251-263.
16. Xu, Q., Johnston, G. C., and Singer, R. A. (1993) *Mol Cell Biol* **13**, 7553-7565.
17. Simic, R., Lindstrom, D. L., Tran, H. G., Roinick, K. L., Costa, P. J., Johnson, A. D., Hartzog, G. A., and Arndt, K. M. (2003) *Embo J* **22**, 1846-1856.
18. Wittmeyer, J., Joss, L., and Formosa, T. (1999) *Biochemistry* **38**, 8961-8971.
19. Holland, P. M., Milne, A., Garka, K., Johnson, R. S., Willis, C., Sims, J. E., Rauch, C. T., Bird, T. A., and Virca, G. D. (2002) *J Biol Chem* **277**, 16229-16240.
20. Roig, J., Mikhailov, A., Belham, C., and Avruch, J. (2002) *Genes Dev* **16**, 1640-1658.

21. Tsay, Y. G., Wang, Y. H., Chiu, C. M., Shen, B. J., and Lee, S. C. (2000) *Anal Biochem* **287**, 55-64.
22. Altschul, S. F., Gish, W., Miller, W., Myers, E. W., and Lipman, D. J. (1990) *J Mol Biol* **215**, 403-410.
23. Altschul, S. F., Madden, T. L., Schaffer, A. A., Zhang, J., Zhang, Z., Miller, W., and Lipman, D. J. (1997) *Nucleic Acids Res* **25**, 3389-3402.
24. Smith, R. F., Wiese, B. A., Wojzynski, M. K., Davison, D. B., and Worley, K. C. (1996) *Genome Res* **6**, 454-462.
25. Gouet, P., Courcelle, E., Stuart, D. I., and Metoz, F. (1999) *Bioinformatics* **15**, 305-308.
26. Sali, A., and Blundell, T. L. (1993) *J Mol Biol* **234**, 779-815.
27. Sippl, M. J. (1993) *Proteins* **17**, 355-362.
28. Keller, D. M., Zeng, X., Wang, Y., Zhang, Q. H., Kapoor, M., Shu, H., Goodman, R., Lozano, G., Zhao, Y., and Lu, H. (2001) *Mol Cell* **7**, 283-292.
29. Keller, D. M., and Lu, H. (2002) *J Biol Chem* **277**, 50206-50213.
30. Eyers, P. A., Erikson, E., Chen, L. G., and Maller, J. L. (2003) *Curr Biol* **13**, 691-697.
31. Jang, Y. J., Ma, S., Terada, Y., and Erikson, R. L. (2002) *J Biol Chem* **277**, 44115-44120.
32. Littlepage, L. E., Wu, H., Andresson, T., Deanehan, J. K., Amundadottir, L. T., and Ruderman, J. V. (2002) *Proc Natl Acad Sci U S A* **99**, 15440-15445.

Figure Legends

Figure 1

Identification of an endogenous FACT-Nek9 multiprotein complex

(A) SSRP1-associated complexes were immunoprecipitated from HeLa nuclear extracts using SSRP1-specific monoclonal antibody 10D1. Specific SSRP1-interacting protein bands that are absent in the control immunoprecipitates were identified by mass spectrometry. In addition to FACT subunits, a ~120 kDa protein was identified as the human Nek9 protein.

(B) Western blot analysis of the different immunoprecipitates targeted by control antibody 2B12, anti-SSRP1 mAbs, 3E4, 10D1, and 7F8, and HeLa cell extracts, as indicated.

Immunoblotting was done using αFACT140 and αSSRP1 (10D1) mAbs (top panel), or αNek9-M antibody (bottom panel). The lower panel schematically represents the approximate regions of SSRP1 (in amino acids) in which the recognition sites of the different monoclonal antibodies may lie, as determined through immunoblotting on deletion constructs of SSRP1.

(C) Western blot analysis of the different immunoprecipitates targeted by αNek9-N (lane1), pre-immune serum (PI, lane 2), and HeLa cell extracts (lane 3). Immunoblotting was done using αFACT140 and αSSRP1 (10D1) mAbs (lower panel), or αNek9-N antibody (top panel).

(D) M2 beads bound without (lane1) or with (lane 2) FLAG-FACT140, or FLAG-p53 (lane 6), and nickel-beads bound without (lane 3) or with (lane 4) His_6-SSRP1, or His_6-Thioredoxin were used as baits in the *in vitro* pull-down assay. Presence and purity of the immobilized proteins were seen on Coomassie blue-stained gels. Lysates from insect cells (Sf9) previously infected with Myc-Nek9-expressing baculoviruses were used in the binding reactions (lanes 1-4). Bound proteins were detected through immunoblotting with anti-Myc antibodies. All proteins, except for the bacterially expressed His_6-Thioredoxin, were derived from baculoviruses-infected insect cells.

(E) Lysates of insect cells (Sf9) singly infected with His_6-SSRP1-expressing baculoviruses (lane 1), or co-infected with FLAG-Nek9-expressing viruses (lane2) were subjected to

immunoprecipitation using the M2 beads (Sigma). Expressions of His_6-SSRP1 (middle panel) and FLAG-Nek9 (lower panel) were monitored by immunoblotting using, respectively, anti-6xHis antibody (Qiagen) and M2 antibody. Components of the M2 immunoprecipitates, as shown by Coomassie blue-stained gel, are as indicated.

(F) Chromatographic fractions (numbers as indicated) generated by the gel filtration of HeLa nuclear extracts (using Sephacryl S-400) were immunoblotted with αFACT140, αSSRP1, and αNek9-M antibodies. Equal amounts of selected fractions were further subjected to immunoprecipitation using mAb 10D1. Immunoprecipitates were also probed with αFACT140, αSSRP1 (10D1), and αNek9-M antibodies.

Figure 2

Subcellular distribution of Nek9 and its cell cycle-dependent colocalization with FACT

(A) Indirect immunofluorescence analysis was performed on asynchronous HeLa cells to observe localization of endogenous Nek9 (a-h), FACT140 (a) and SSRP1 (b-h), respectively using αNek9-M antibody, αFACT140 mAb 8D2, and αSSRP1 mAb 10D1. Nuclear DNA was counter-stained by DAPI. Cells in different phases of the cell cycle were examined: interphase (a and b), metaphase (c and d), anaphase (e), telophase/cytokinesis (f), and G_0/G_1 phase (g and h). Individual and merged images were generated by a Zeiss LSM 510 laser scanning confocal microscope.

(B) HeLa cells ectopically expressing FLAG-Nek9 were stainined with αFLAG mAb and counter-stained with DAPI. Images shown in (a) are an example of localization of FLAG-Nek9 in the nucleus. A few FLAG-Nek9-positive cells also exhibited nucleocytoplasmic or cytoplasmic staining signals (b).

Figure 3

Upon autoactivation *in vitro*, Nek9 undergoes phosphorylation on the conserved Thr_{210} and phosphorylation-dependent electrophoretic mobility shift

(A) An alignment of the kinase domain of Nek9 with those of human Aurora-2 kinase (accession no.1MUO), porcine cAMP-dependent protein kinase (CaPK, #1CDK), rat calmodulin-dependent protein kinase (CalmPK, #1A06), and human PAK-1 (#1F3M). Homologous amino acid residues are highlighted in red blocks with white characters, and similar residues are within blue boxes. Secondary structure assignments from the Aurora-2 crystal structure are shown above the aligned sequences with blue symbols: α, α-helix; β, β-sheet; η, 3_{10}-helix; T, turn. Amino acid residues important for catalysis are also indicated from below (numbers corresponding to the Aurora-2 sequence): K31 (arrowhead), D125/N130 (circles), and T157 (star).

(B) Molecular modeling of the Nek9 kinase domain. Side chains of the residues important for catalysis (K81, D176, and N181) as well as Thr_{210} are depicted with ball-and-stick

representation. Arrows indicate the location of the Thr_{210} residue and the activation loop region. A phosphate moiety was added on the threonine, and its surface potential is represented by a transparent hemisphere. A magnified view of the catalytic site is shown on the right.

(C) An alignment of the activation loop region of Nek9 with those of the other Nek family members. The conserved Thr_{210} residues are highlighted in blue blocks with white characters, and other conserved residues within this region are in red characters.

(D) Endogenous Nek9 was immunoprecipitated from HeLa cells by αNek9-M antibody (lanes 1-3) and subjected to kinase assay (autoactivation) with the indicated concentrations of ATP. Immunoprecipitates were immunoblotted with either αNek9-M antibody (top panel) or αphospho-Thr_{210} antibody (middle panel), or were further washed and incubated with [^{32}P]ATP and histone H1 (1 μg) at 30℃. Phosphate incorporation on histone H1 was monitored by ^{32}P autoradiography (bottom panel). Arrowheads indicate the positions of the lower-mobility form, whereas the asterisks point to the unactivated form of Nek9.

(E) Endogenous Nek9 was immunoprecipitated from HeLa cells by αNek9-M antibody. Immunoprecipitates were washed and incubated without (lane 1), or with 100 μM of ATP (lanes 2 and 3). After autoactivation, immunoprecipitates were further subjected to buffer (lanes 1 and 2) or alkaline phosphatase treatment (lane 3). All immunoprecipitates were resolved by SDS-PAGE, followed by Western blot using αNek9-M antibody (upper) or

αphospho-Thr_{210} antibody (lower). Arrowheads designate the positions of phospho-Nek9, while asterisks denote the Nek9 with usual mobility. In the right panel, the electrophoretic mobility of the autoactivated species (lane 4) was compared to that of Nek9 immunoprecipitated from exponentially growing cells (lane 5), and M-phase cells (lane 6). Black arrowheads, asterisks, and gray arrowhead respectively designate the activated form, the unactivated form, and the mitotic form.

Figure 4

Phospho-Nek9 associates with FACT in a cell cycle-dependent manner

(A) HeLa cells were immunoprecipitated with the indicated antibodies: control antibody (lane 2), αSSRP1 mAb 10D1 (lane 3), rabbit pre-immune sera (lane 4), and αNek9-M antibody (lane 5) (cell extract input is shown in lane 1). The presence of Nek9, FACT heterodimers, and phospho-Nek9 was detected by Western blot analysis using αNek9-M antibody (top), αFACT140 and αSSRP1 antibodies (middle), and αphospho-Thr_{210} antibody (bottom), respectively. Position of the upshifted, phosphorylated Nek9 is indicated by the upper arrow, whereas the lower arrow point to the presumed usual location of Nek9.

(B) FACT-associated immunocomplex was isolated by αSSRP1 mAb 10D1 from HeLa cells at different cell cycle stages: exponentially growing (lanes 1 and 5), G_1/S phase (lane 2), S phase at 1 hr after double-thymidine block (lane 3), S phase at 3 hr (lane 4), and M phase

(lane 6) and G_2 (lane 7). The presence of Nek9, FACT heterodimers, and phospho-Nek9 was detected by αNek9-M antibody (top), αFACT140 and αSSRP1 antibodies (bottom), and αphospho-Thr_{210} antibody (middle), respectively. The arrowhead designates the location of the Thr_{210}-phosphorylated form of Nek9. The graph on the bottom illustrates the changes in the degree of Thr_{210} phosphorylation (on FACT-associated Nek9) across different phases. The degree of phosphorylation, expressed as a ratio in band intensity of phopho-Nek9 to total Nek9, was normalized to the asynchronous group.

Figure 5

RNAi ablation of endogenous Nek9 results in slower cellular growth

(A) Equal loadings of whole cell extracts derived from HeLa cells stably harboring control-RNAi (control 1 and control 2), or Nek9-targeting dsRNA (clone 1 and clone 2) were resolved by SDS-PAGE and blotted with αNek9-M antibody (indicated by arrowhead). Asterisk denotes α-tubulin.

(B) Cell proliferation of the generated control and $Nek9^{RNAi}$ stable cells was determined by colony formation assay, as described in Materials and methods.

Figure 6

Slower growth of $Nek9^{RNAi}$ cells can be partly attributed to prolonged G_1 and S phases

(A) Cells stably harboring control or Nek9-targeting dsRNA were synchronized at G_2/M as described in Materials and methods. Cell cycle progression was analyzed based on DNA content by FACS.

(B) Control and $Nek9^{RNAi}$ cells were synchronized at the G_1/S junction by double thymidine block. At the indicated time points after the release, cells were harvested and subjected to DNA content analysis by FACS.

(C) Control and $Nek9^{RNAi}$ cells were synchronized at the G_1/S junction, and pulse-labeled with BrdUTP before being harvested at different time points as in (B). Cell cycle profiles and degree of BrdU labeling (i.e. active DNA replication) were monitored by FACS. The "labeling index" quantitatively represents the percentage (%) of BrdU-positive cells in a counted pool of cells.

Figure 1A

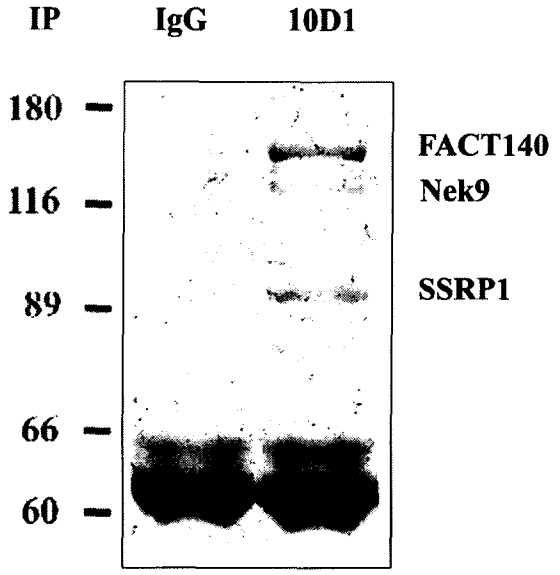

Figure 1B

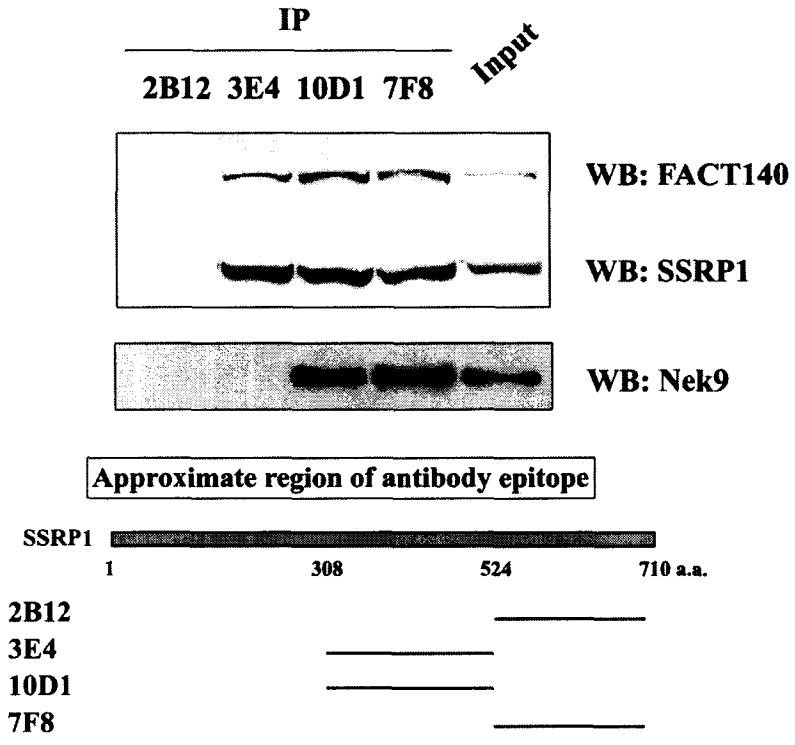

Figure 1C

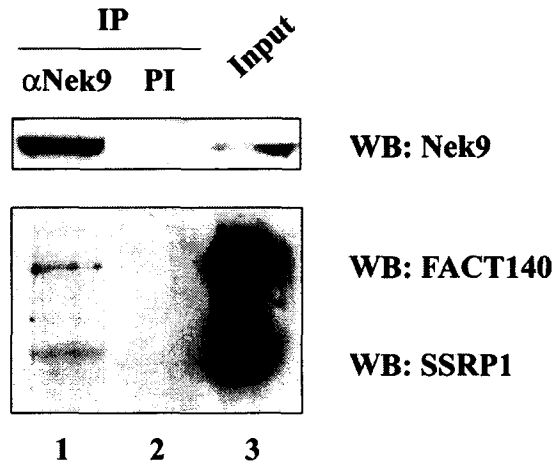

Figure 1F

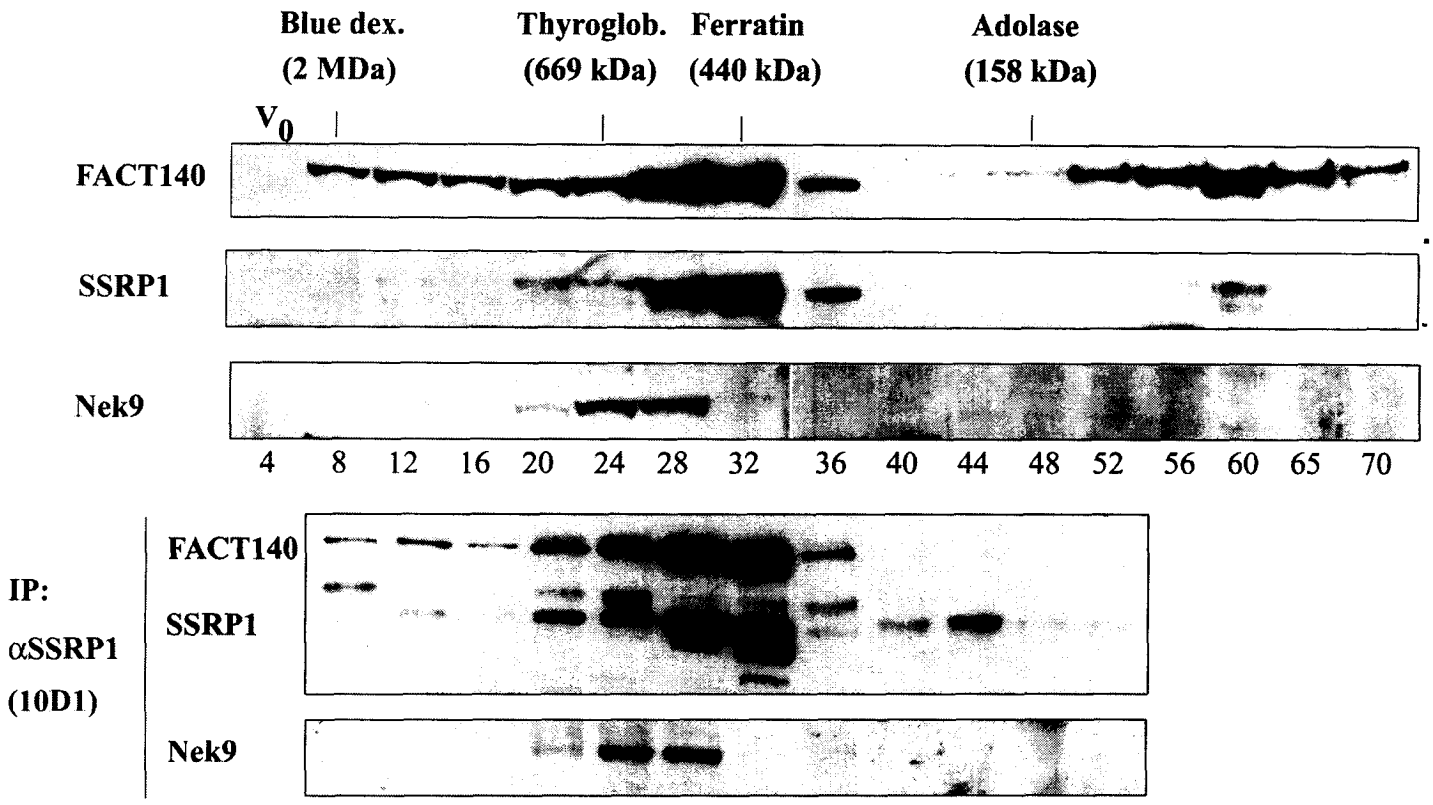

Figure 1D

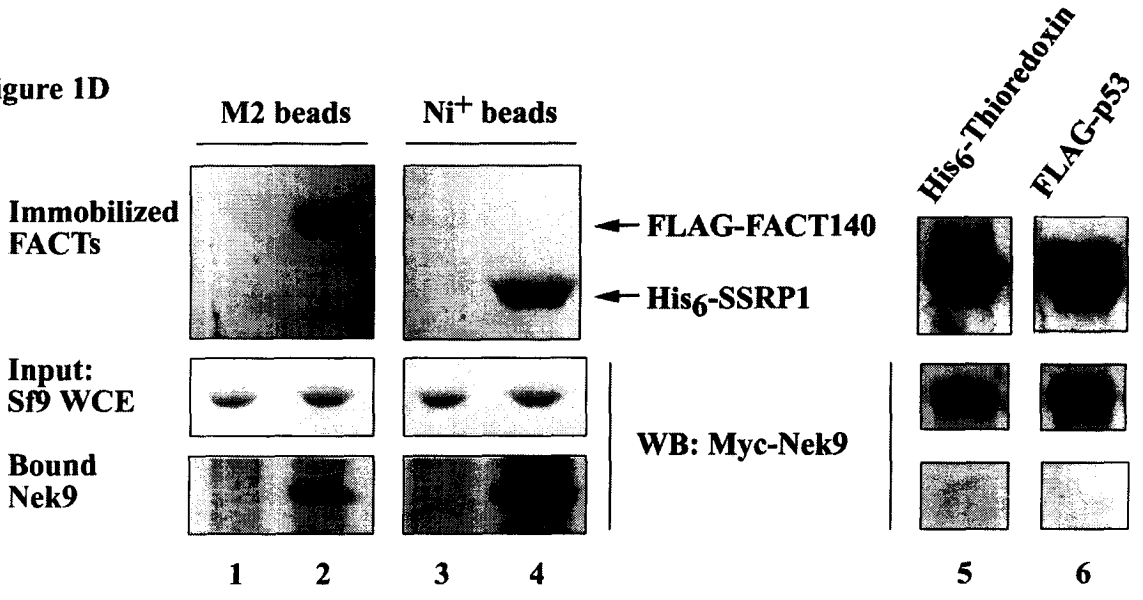

Figure 1E

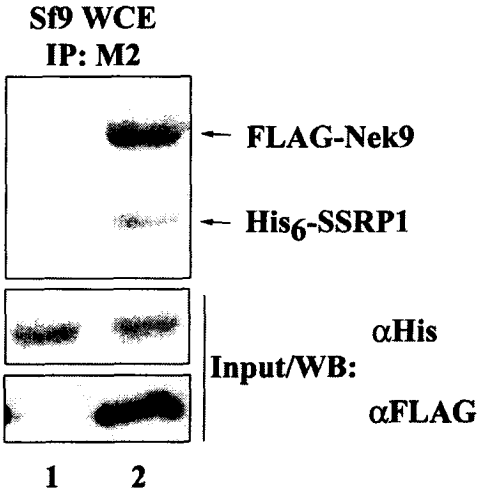

Figure 2A

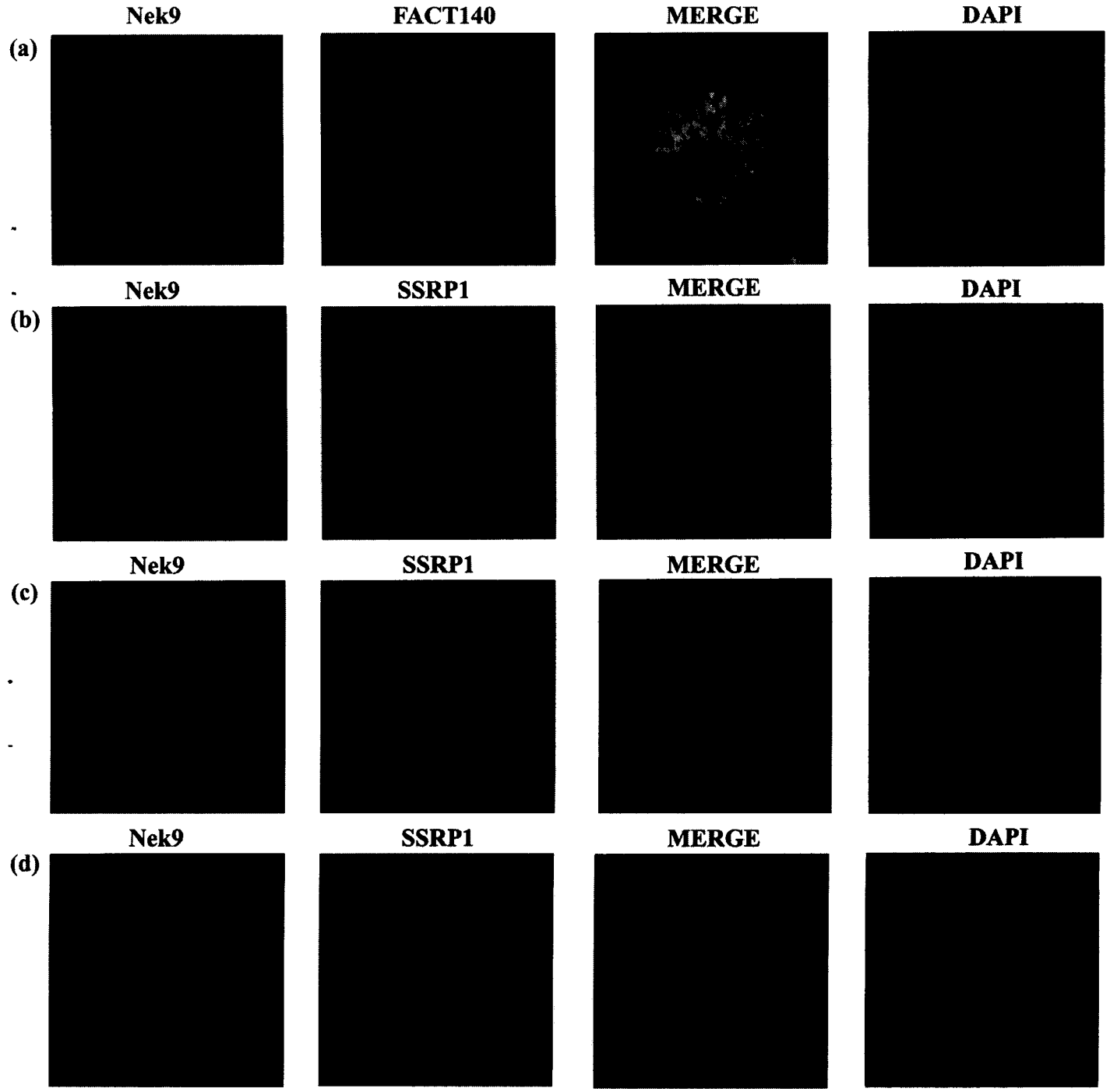
Nek9
FACT140
MERGE
DAPI
(a)
Nek9
SSRP1
MERGE
DAPI
(b)
Nek9
SSRP1
MERGE
DAPI
(c)
Nek9
SSRP1
MERGE
DAPI
(d)

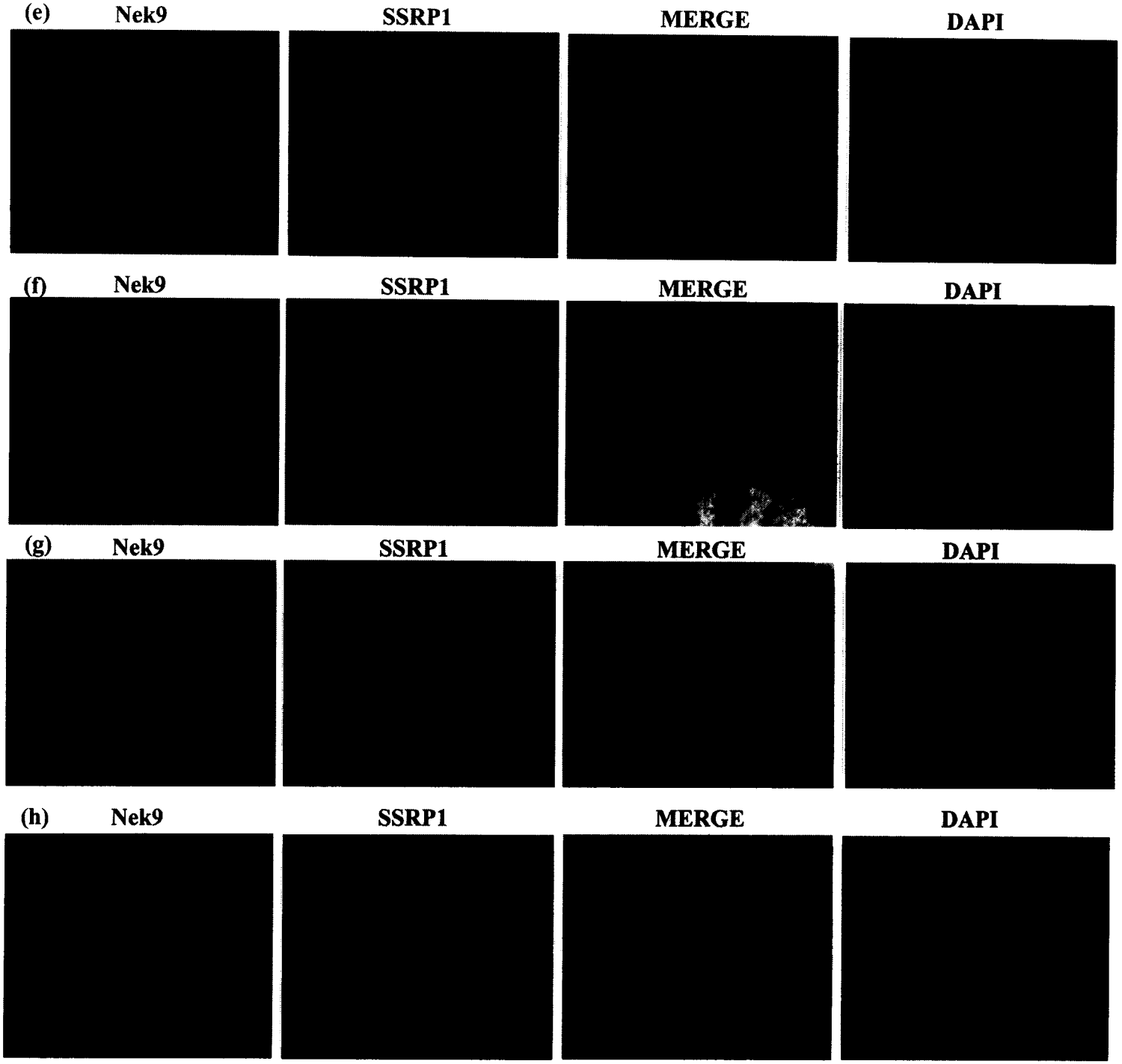
(e)
Nek9
SSRP1
MERGE
DAPI
(f)
Nek9
SSRP1
MERGE
DAPI
(g)
Nek9
SSRP1
MERGE
DAPI
(h)
Nek9
SSRP1
MERGE
DAPI

Figure 2B

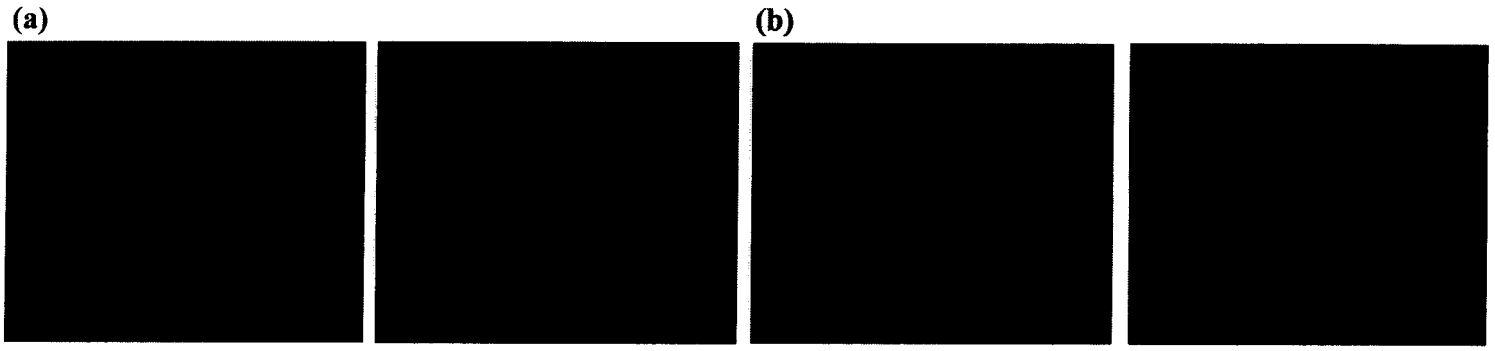
(a)
(b)

Figure 3A

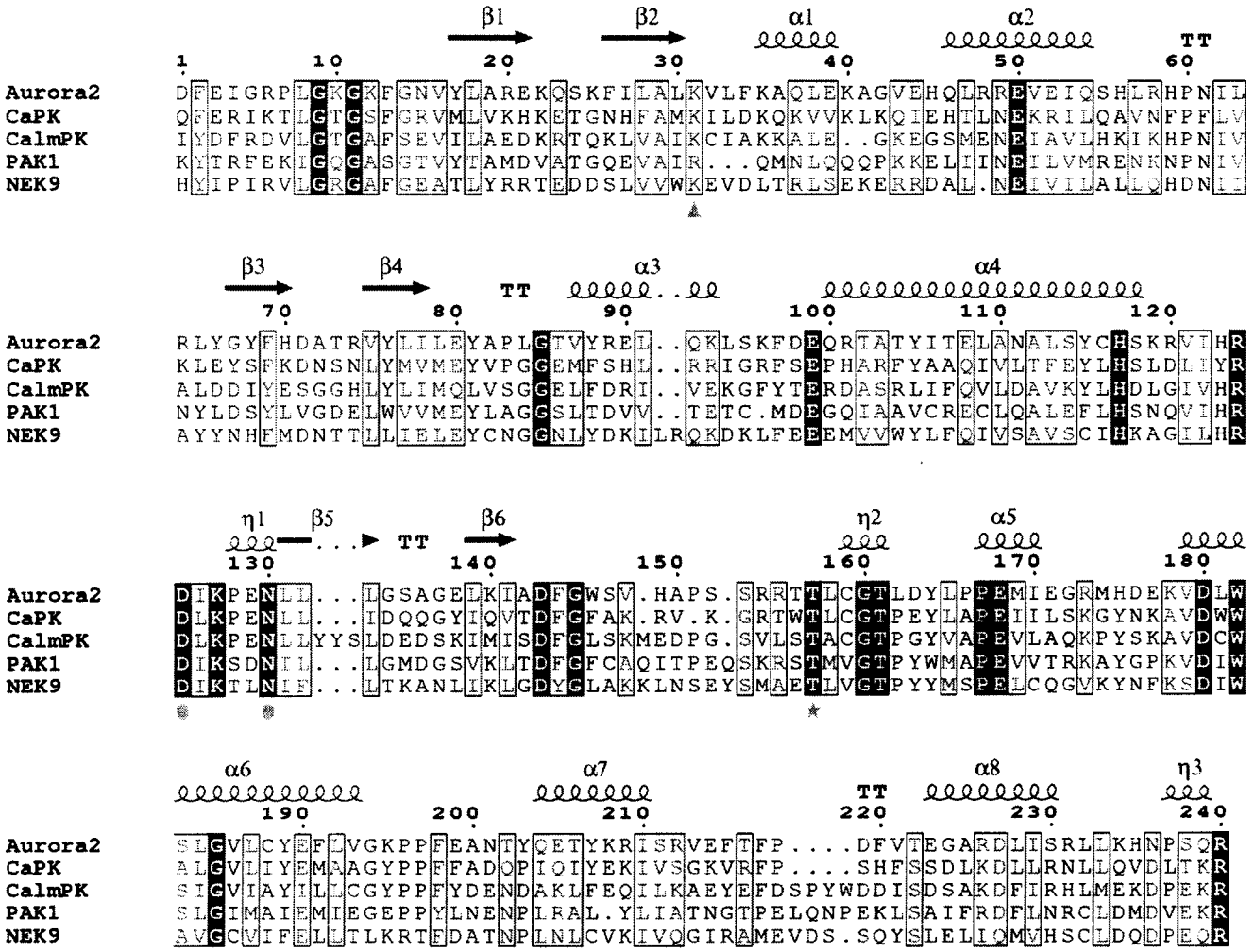

Figure 3B

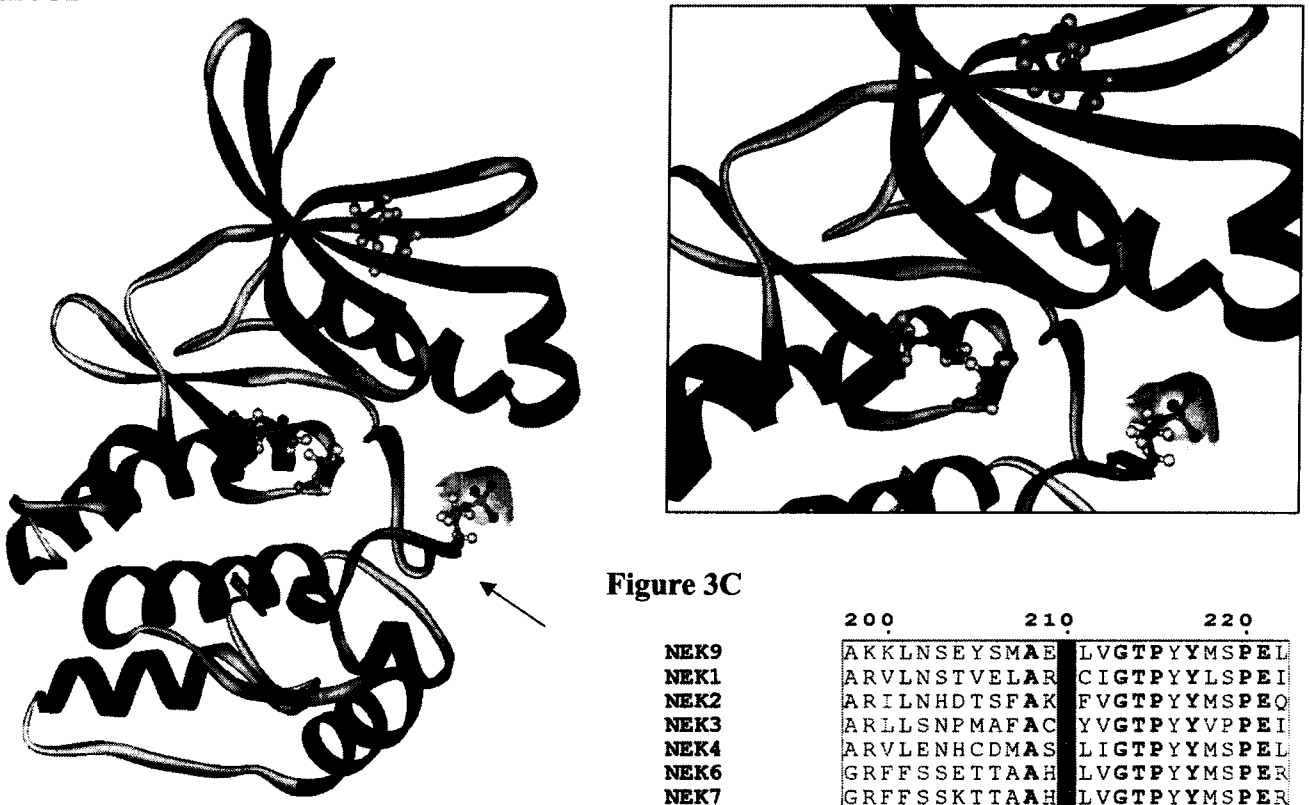

Figure 3C

Figure 3D

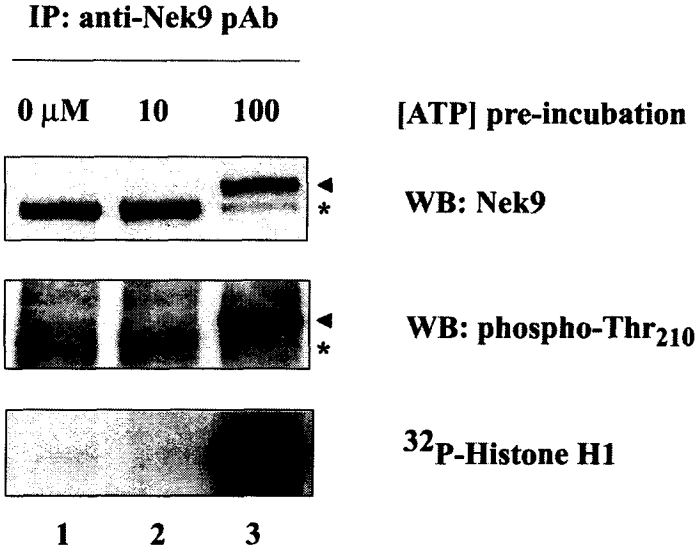

Figure 3E

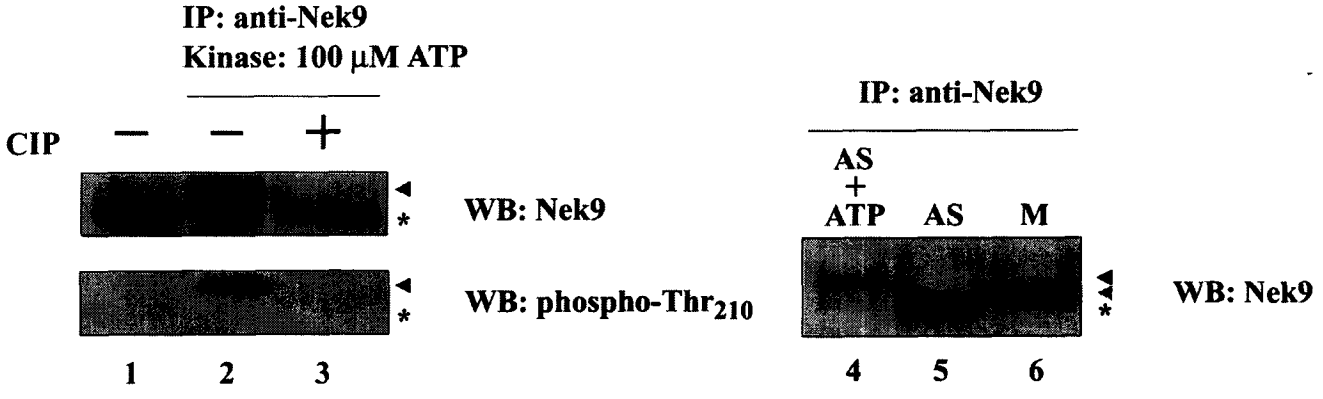

Figure 4A

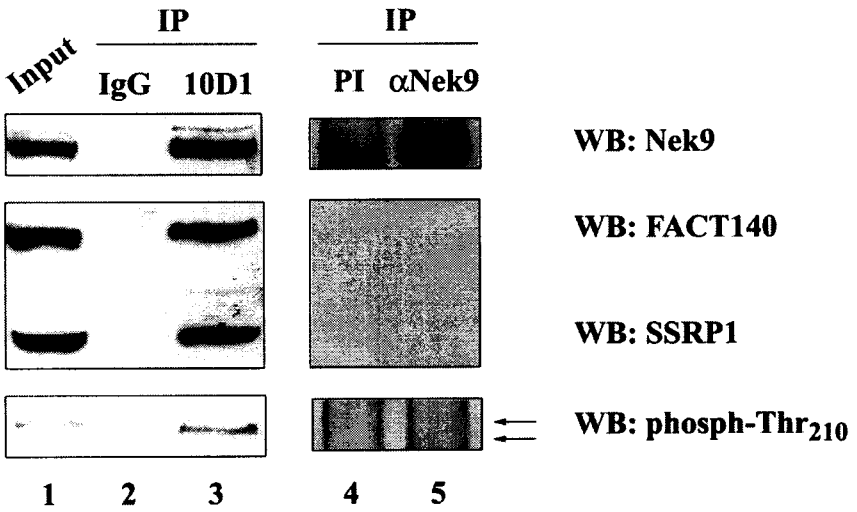

Figure 4B

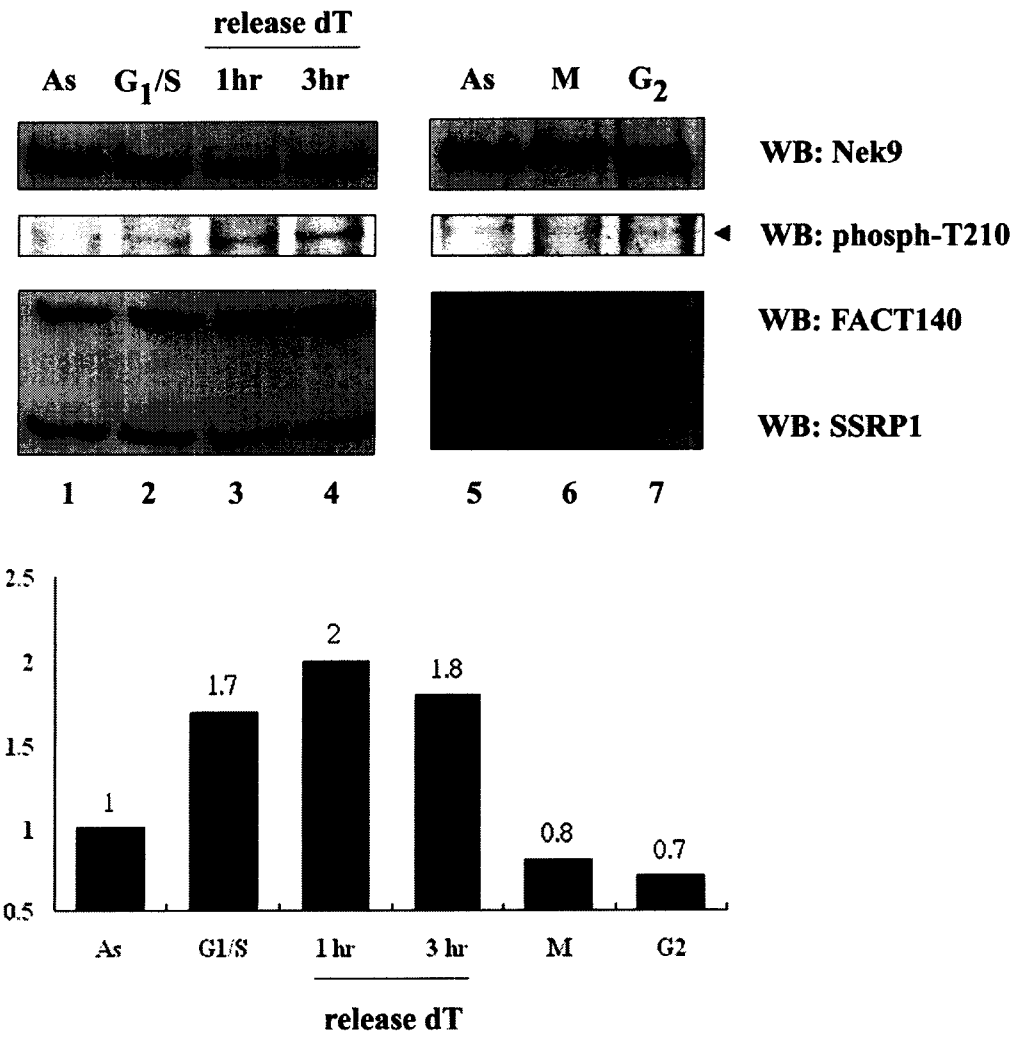

Figure 5A

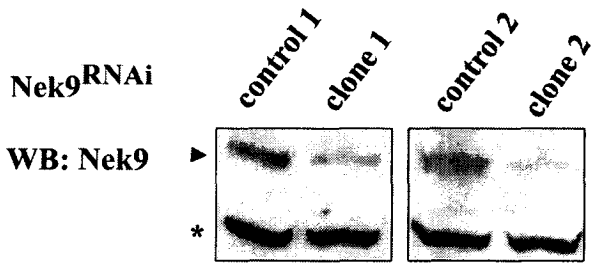

Figure 5B

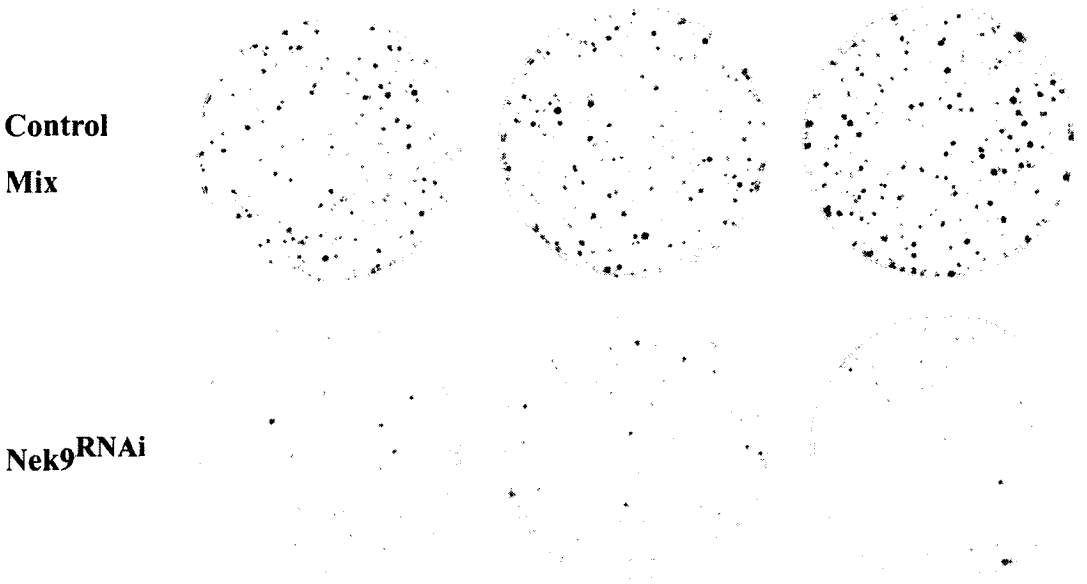

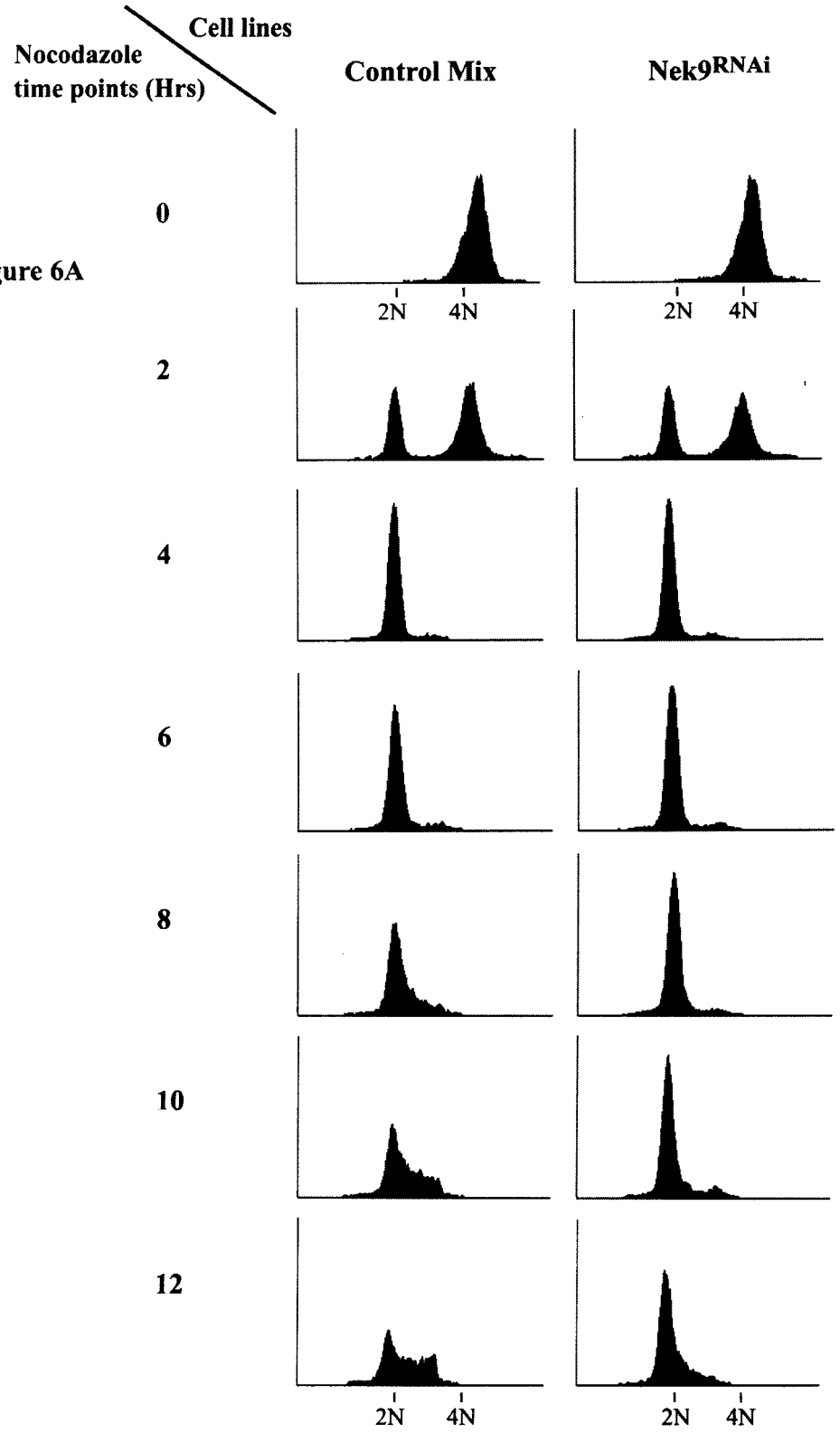
Cell lines
Nocodazole time points (Hrs)
Control Mix
Nek9RNAi
0
2
4
6
8
10
12
2N
4N
2N
4N
2N
4N
2N
4N

Figure 6A

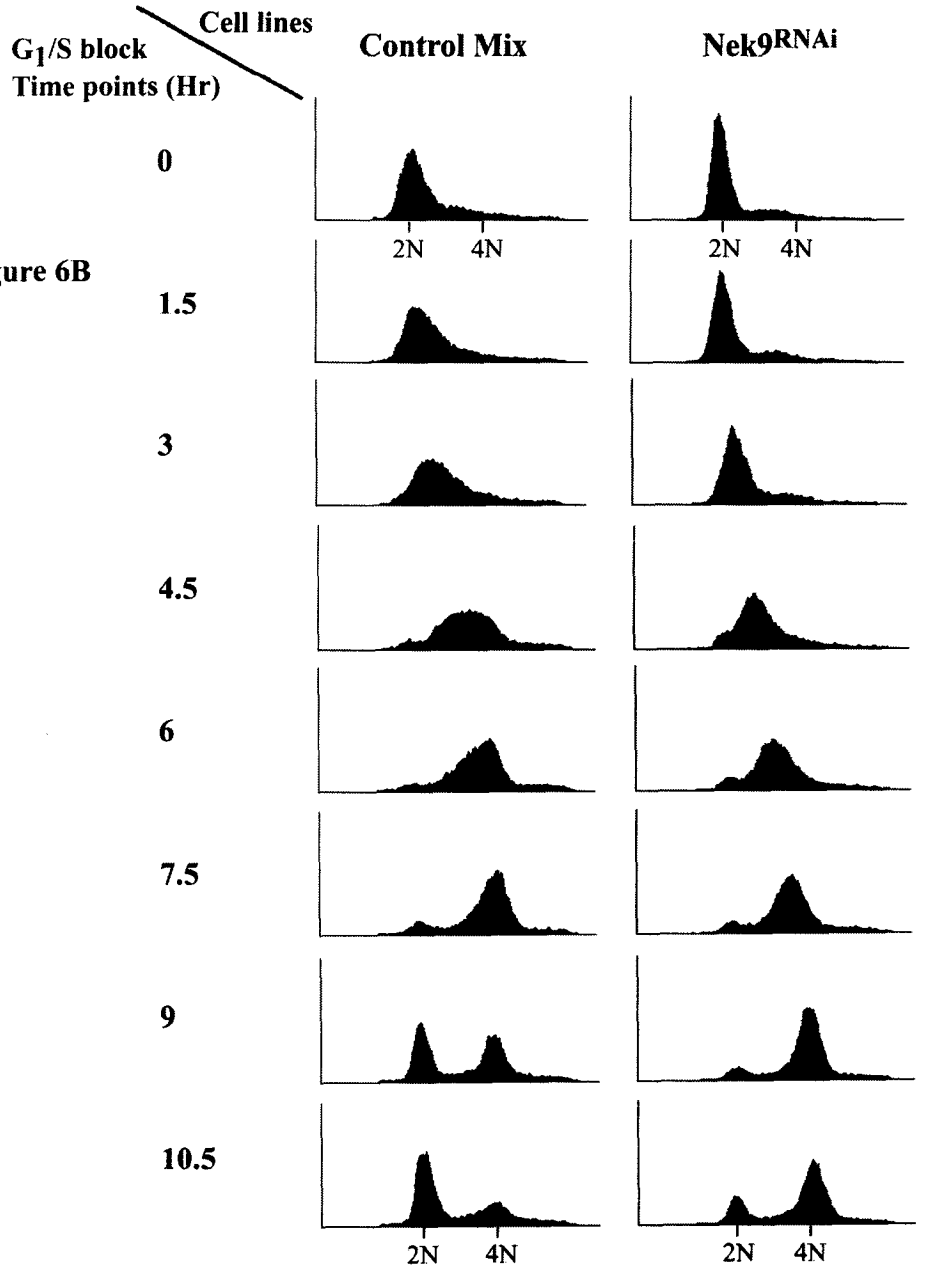

Figure 6B

Figure 6C

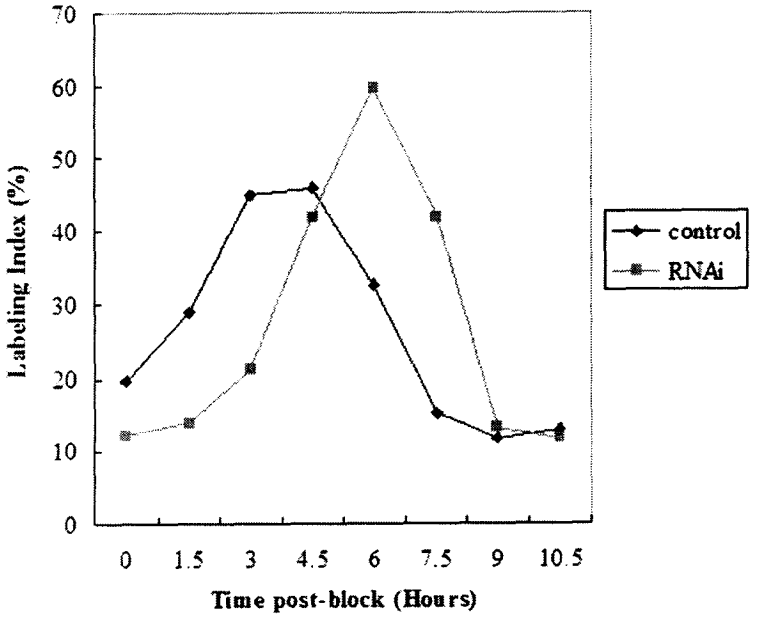

balt3/bc-bc/bc-bc/bc0104/bc9124-04g | stafford S=3 | 5/11/03 4:39 | Comments: | ARTNO: M305501200

THE JOURNAL OF BIOLOGICAL CHEMISTRY Vol. 279, No. ??, Issue of ???? ??, pp. 1–xxx, 2004

Printed in U.S.A.

Differential Activation of a C/EBPβ Isoform by a Novel Redox Switch May Confer the Lipopolysaccharide-inducible Expression of Interleukin-6 Gene*

Received for publication, May 27, 2003, and in revised form, October 3, 2003
Published, JBC Papers in Press, October 6, 2003, DOI 10.1074/jbc.M305501200

Wen-Chi Su‡§, Han-Yi Chou‡§, Ching-Jin Chang¶, Yu-May Lee¶, Wei-Hao Chen‡, Kuo-Hsiang Huang‡, Ming-Yue Lee‡, and Sheng-Chung Lee‡¶‖**

AQ: A *From the Institutes of ‡Molecular Medicine and ‖Clinical Medicine, College of Medicine, National Taiwan University and the ¶Institute of Biological Chemistry, Academia Sinica, Taipei, Taiwan*

AQ: B **C/EBPβ, a member of the C/EBP family, is one of the key transcription factors responsible for the induction of a wide array of genes, some of which play important roles in innate immunity, inflammatory response, adipocyte and myeloid cell differentiation, and the acute phase response. Three C/EBPβ isoforms (*i.e.* LAP*, LAP, and LIP) were known to arise from differential translation initiation and display different functions in gene regulation. C/EBPβ is known to induce interleukin (IL)-6 gene when P388D1 cells are treated with lipopolysaccharide (LPS). Exactly how the transcriptional activities of C/EBPβ isoforms are involved in the regulation of the IL-6 gene remains unclear. Here we report that LPS-induced expression of IL-6 gene in P388D1 cells is mediated by a redox switch-activated LAP*. The intramolecular disulfide bonds of LAP* and LAP have been determined. Among the cysteine residues, amino acid 11 (Cys^{11}) of LAP* plays key roles for determining the overall intramolecular disulfide bonds that form the basis for redox switch regulation. The DNA binding activity and transcriptional activity of LAP* are enhanced under reducing condition. LAP and LIP, lacking 21 and 151 amino acids, respectively, in the N-terminal region, are not regulated in a similar redox-responsive manner. Our results indicate that LAP* is the primary isoform of C/EBPβ that regulates, through a redox switch, the LPS-induced expression of the IL-6 gene.**

AQ: C

AQ: D Members of the C/EBP[1] family of proteins have been implicated in the differentiation of myelomonocytic cells and the regulation of gene expression during activation of macrophages (1, 2). Regulation of macrophage gene expression by lipopolysaccharide (LPS) is of potential importance in the pathogenesis of infection, inflammation, and septic shock. A detailed understanding of the molecular basis of such disease requires a thorough analysis of the mechanisms by which the actions of LPS are transduced to the nucleus to alter gene expression. The expression of C/EBPβ is inducible in monocytes and macrophages by LPS. C/EBPβ has been implicated in the regulation of proinflammatory cytokines as well as other genes associated with macrophage activation and the acute phase response (3, 4). The promoter regions of the genes for IL-6, TNFα, IL-1, IL-8, and granulocyte colony-stimulating factor contain C/EBPβ-binding sites (3, 5–7). The stable expression of C/EBPβ in a murine P388 lymphoblast cell line is sufficient to confer LPS-inducible IL-6 expression (8, 9). Conversely, inhibition of endogenous C/EBPβ expression by antisense RNA interference blocks LPS induction of IL-6 expression in the murine P388D1(IL1) macrophage-like cells (8). C/EBPβ can also activate the proximal promoter of the human TNF-α gene in RAW264.7 monocytic cells, whereas overexpression of a dominant negative C/EBPβ inhibits LPS-induced activation (10). In the murine P388D1(IL1) cell line, C/EBPβ is constitutively expressed, and IL-6 and TNF-α can readily be induced by agents such as LPS. The exact molecular mechanisms of LPS stimulation of IL-6 and TNF-α gene expression and how this relates to C/EBPβ-mediated activation of these genes remain unclear.

AQ: E

Structurally, members of C/EBP family are bZIP proteins with sequence-specific DNA binding activity when homo- or heterodimerized. The DNA-binding and transactivation domains are located in the C- and N-terminal regions, respectively (11). The intronless *c/ebpβ* gene (also known as *lap* in rat, *agp/ebp* in mouse, and NF-IL6 in human) encodes three isoforms, including two activators (termed LAP* and LAP, respectively) and a repressor (*i.e.* LIP). These isoforms of C/EBPβ are differentially translated from the same mRNA (12). The expression of these isoforms is developmentally and hormonally regulated (12–14).

The functional differences between the two activator isoforms, LAP* and LAP, have been addressed in two examples (15, 16). The 21 amino acids of the N terminus region of LAP* are responsible for its functional interaction with NF-κB and for recruiting to the SWI-SNF complex involved in chromatin remodeling. Both NF-κB and C/EBPβ can activate the inflammatory cytokine genes, and conversely, these cytokines can induce NF-κB and C/EBPβ (17). These results suggest that the mechanisms for activating C/EBPβ and NF-κB may converge on a post-translational level. There is a cysteine residue, Cys^{11}, located in the 21-amino acid stretch of the N-terminal region of LAP*. The possibility of Cys^{11} involved in the tertiary structure

AQ: F

* This work was supported by National Science Council Grants NSC 90-2321-B002-003 and NSC92-2320-B002-188 and by funds from the Institute of Biological Chemistry, Academia Sinica, Taiwan. The costs of publication of this article were defrayed in part by the payment of page charges. This article must therefore be hereby marked "*advertisement*" in accordance with 18 U.S.C. Section 1734 solely to indicate this fact.

§ These authors contributed equally to this work.

** To whom correspondence should be addressed: Institute of Molecular Medicine, National Taiwan University, #7, Chung Shan South Rd., AQ: I NTUH, Taipei, Taiwan. Tel.: 886-2-2356-2982; Fax: 886-2-2321-0977; E-mail: slee@ccms.ntu.edu.tw.

[1] The abbreviations used are: C/EBP, —; LPS, lipopolysaccharide; IL, interleukin; TNF, tumor necrosis factor; PDTC, pyrrolidine dithiocarbamate; NAC, *N*-acetylcysteine; CAT, chloramphenicol acetyltransferase; DTT, dithiothreitol; HPLC, high pressure liquid chromatography; AQ: J ChIP, chromatin immunoprecipitation; IGF, insulin-like growth factor; IGFBP, IGF-binding protein.

or redox sensing that results in the differential activation of LAP* and LAP deserves to be investigated.

The activities of transcription factors may be regulated in a redox-sensitive manner. LPS has been shown to induce changes in cellular redox states. The cellular levels of thioredoxin, thioredoxin reductase, and NADPH, as well as the reactive oxygen species, may be elevated by LPS treatment (18–20). Redox-based transcriptional regulation has been studied extensively in prokaryotes (21–24) and demonstrated in eukaryotic cells (25–31). Among the redox-sensing proteins, thioredoxin, thioredoxin reductase, and other related oxidoreductases are involved in the regulation of activities of many key proteins in species ranging from bacteria to eukaryotic cells. REF-1 has been characterized as a factor that imparts strong DNA binding activity to the AP-1 complex by maintaining the cysteines as reduced sulfhydryl groups (32). The DNA binding activity of transcription factors can be affected by redox modifications (25, 27, 29, 33). Cysteine residues of several transcription factors, although not directly involved in DNA binding, modulate DNA binding activity in response to the cellular redox states (25–27, 33–37).

There are six, five, and two cysteines in LAP*, LAP, and LIP, respectively. To address the potential regulation of LAP* and LAP activity by LPS, we performed detailed biochemical and functional studies on the differential regulation of LAP* and LAP. Here we report that only LAP* is activated by LPS-induced redox switch. Upon reduction, LAP* is activated to up-regulate the transcription of IL-6 gene in P388D1(IL1) cells. We have determined that disulfide bonds formed in LAP* and LAP. A cysteine residue located in the N-terminal 21-amino acid region plays key roles in determining the tertiary structure and the redox-regulated activation of LAP*. The importance and the biological significance of this discovery are discussed.

EXPERIMENTAL PROCEDURES

Cell Culture and Transient Transfection—293T cells were cultured in Dulbecco's modified Eagle's medium (Invitrogen) supplemented with 10% fetal calf serum (Hyclone). P388D1(IL1) cells were cultured in Iscove's modified Dulbecco's medium (Invitrogen) supplemented with 10% fetal calf serum and 2 mM L-glutamine (Invitrogen). Both cultures were supplemented with 100 units/ml penicillin and 100 μg/ml streptomycin. All nuclear extracts from 293T or P388D1(IL1) cells were fresh prepared with nitrogen gas. Transient transfection of 293T cells was performed with a calcium phosphate precipitation method. The calcium phosphate-plasmid DNA precipitate contained, in each well of a 6-well plate, 1 μg of AGP-CAT, 0.3 μg of pSV-β-galactosidase, and various constructs of pCMV-C/EBPβ (detailed in the legend of figures). pCMV plasmid DNA was used to give a final amount of 2 μg of DNA for each transfection. 20 h post-transfection, the cultures were replaced with fresh medium and treated with either 10 μM pyrrolidine dithiocarbamate (PDTC) or 1 mM *N*-acetylcysteine (NAC) for 16 h. The cells were harvested, and CAT activity was determined and normalized with β-galactosidase activity. At least two independent, duplicate experiments were performed to each assay.

Plasmids—The AGP-CAT and pCMV-C/EBPβ plasmids were obtained as described elsewhere (38). FLAG-tagged LAP*, LAP, and LIP constructs were obtained by cloning the full-length and the respective N-terminal deletion constructs into pCMV-tag2 expression vector (Stratagene). Mutants of each of the six cysteine residues (*i.e.* Cys → Ser) were generated with the M13mp18 site-directed mutagenesis system (Promega) using the following synthetic primers: C11S, 5′-ACGCAGCAAGCCTCCCG-3′; C33S, 5′-AGCCCGACAGCCTGGAA-3′; C123S, 5′-CCGCCCGCAAGCTTTCCG-3′; C143S, 5′-CCGCGGACAGCAAGCGC-3′; C201S, 5′-CCCGCCGCAAGCTTCGCG-3′; and C296S, 5′-CGGGCCACAGCTAGCGCGGCGCG-3′. The mutated nucleotides are underlined. The mutated cDNAs were then cloned into pCMV-tag vector.

Antibodies—18F8 monoclonal antibody was produced from hybridomas generated by fusing splenocytes from BALB/c mouse immunized with MHRLLAWDAACLPPPAAFPKLH with myelomas. 1H7 monoclonal antibody was obtained by immunizing BALB/c mice with recombinant LIP. A16 and other antibodies were described previously (15).

Chromatin Immunoprecipitation Assays—Chromatin immunoprecipitation assays were modified from previously described methods (39). Briefly, P388D1 cells were cross-linked with 1% formaldehyde for 10 min at 37 °C. The nuclei were isolated and sonicated into oligonucleosomes of ~600 bp in length. The sheared chromatin was immunoprecipitated with 18F8 and 1H7 antibodies overnight, followed by 1 h of incubation with protein G-agarose, cross-linking reversal, and deproteination. The presence of immunoprecipitated DNA was detected by PCR with the following primers: IL-6, sense, 5′-GCTTCTTAGGGCTAGCCTCA-3′, and antisense, 5′-AGCTACAGACATCCCCAGTC-3′; TNF-α, sense, 5′-TTCCGAGGGTTGAATGAGAGCT-3′, and antisense, 5′-TTTCTGTTCTCCCTCCTGGCTA-3′; and C/EBPβ, sense, 5′-GTAGCTGGAGGAACGATC3′, and antisense, 5′-TCGGGAACACGGAGGAGC-3′. PCR was performed for 25 cycles. The products were resolved by 2% agarose gels and visualized with ethidium bromide staining. UV-illuminated images were photographed and analyzed by AlphaImager 1220 (Alpha Innotech Corp.)

Northern Blot Analysis—P388D1(IL1) cells were cultured to 80% confluent and stimulated with 1 μg/ml LPS (*Escherichia coli* 0111:B4; Sigma). The total RNA was extracted with TRIZOL reagent (Invitrogen). Approximately 10 μg of total cellular RNA of each sample was separated by electrophoresis in a 1% agarose gel and analyzed by Northern blotting according to standard protocols. IL-6 probe was generated by reverse transcription-PCR from P388D1(IL1) RNA with the following primers: IL-6 forward primer, 5′-ATGAAGTTCCTCTCTGCAAGAG-3′, and IL-6 reverse primer, 5′-CTAGGTTTGCCGAGTAGATCTCA-3′. Full-length cDNA was used to probe C/EBPβ RNA as described previously (4).

Alkylation of Free Thiol Groups with Iodoacetamide in Vivo—The alkylation method was performed as described previously (40). P388D1(IL1) cells were stimulated with 1 μg/ml LPS in the presence of 0.1 mM iodoacetamide (Sigma) to prevent free thiol groups from oxidizing to disulfide. Direct lysates were prepared at the indicated times with SDS sample dye containing 200 mM iodoacetamide at room temperature. The lysates were then resolved by nonreducing SDS-PAGE followed by Western blot analysis.

Electrophoretic Mobility Shift Assay—The specific probe for C/EBPβ was prepared by annealing the oligonucleotides 5′-GATCATTTTGTGTAAGAC-3′ and 5′-GATCGTCTTACACAAAAT-3′. The probe was labeled with T4 polynucleotide kinase and [γ-^{32}P]ATP. Nuclear extract (5–10 μg) from P388D1(IL1) cells or transfected 293T cells was incubated with the probe (1 ng) and 300 ng poly(dI-dC) in either the absence or presence of DTT, NADPH (Sigma), thioredoxin (Sigma), or the combination of NADPH, thioredoxin, and thioredoxin reductase (Sigma) at 37 °C for 20 min. For supershift assay, after the reaction mixture was incubated, 1–2 μl of anti-C/EBPβ antibody was added, and the incubation continued at room temperature for additional 20 min. The reaction mixtures were separated by 5% PAGE in Tris/glycine/EDTA buffer.

Disulfide Bond Determination by LC ESI Mass Spectrometry—FLAG-C/EBPβ isoforms were expressed in 293T cells, immunoprecipitated by M2 beads, and resolved in SDS-PAGE under nonreducing conditions. The in-gel tryptic digest of C/EBPβ was dissolved in 0.1% formic acid, separated with an ABI 140D HPLC (Perkin-Elmer, 150 × 0.5 mm Brownlee reversed phase C18 column packed with 5-μm particles with a 300-Å pore), and on-line detected with a Finnigan Mat LCQ ion trap mass spectrometer. The mobile phase of HPLC consisted of various mixing ratios of 0.1% aqueous formic acid (solution A) and 0.1% formic acid in acetonitrile (solution B). The HPLC analysis was run using a gradient: 5% B for the first 25 min, 5–15% B in 25–30 min, 15–50% B in 30–100 min, and 50–65% B in 100–105 min; this final isocratic solvent was used until all of the peptides were eluted. The eluted peptides were analyzed under positive ion mass spectrometry scan mode over an *m/z* range of 395–1605. A table of detected masses was generated from the acquired mass spectra by the SEQUEST Browser software (Finnigan). The acquired ion masses were then manually examined for possible combinations of peptides containing cysteine residues.

AQ: G

AQ: H

RESULTS

LAP Is Recruited to IL-6 Gene Promoter after LPS Treatment*—Schematic representation of the C/EBPβ isoforms is shown in Fig. 1*A*. There are six cysteine residues in the mouse LAP* (*i.e.* Cys^{11}, Cys^{33}, Cys^{123}, Cys^{143}, Cys^{201}, and Cys^{296}), five in LAP (*i.e.* Cys^{33}, Cys^{123}, Cys^{143}, Cys^{201}, and Cys^{296}), and two

F1

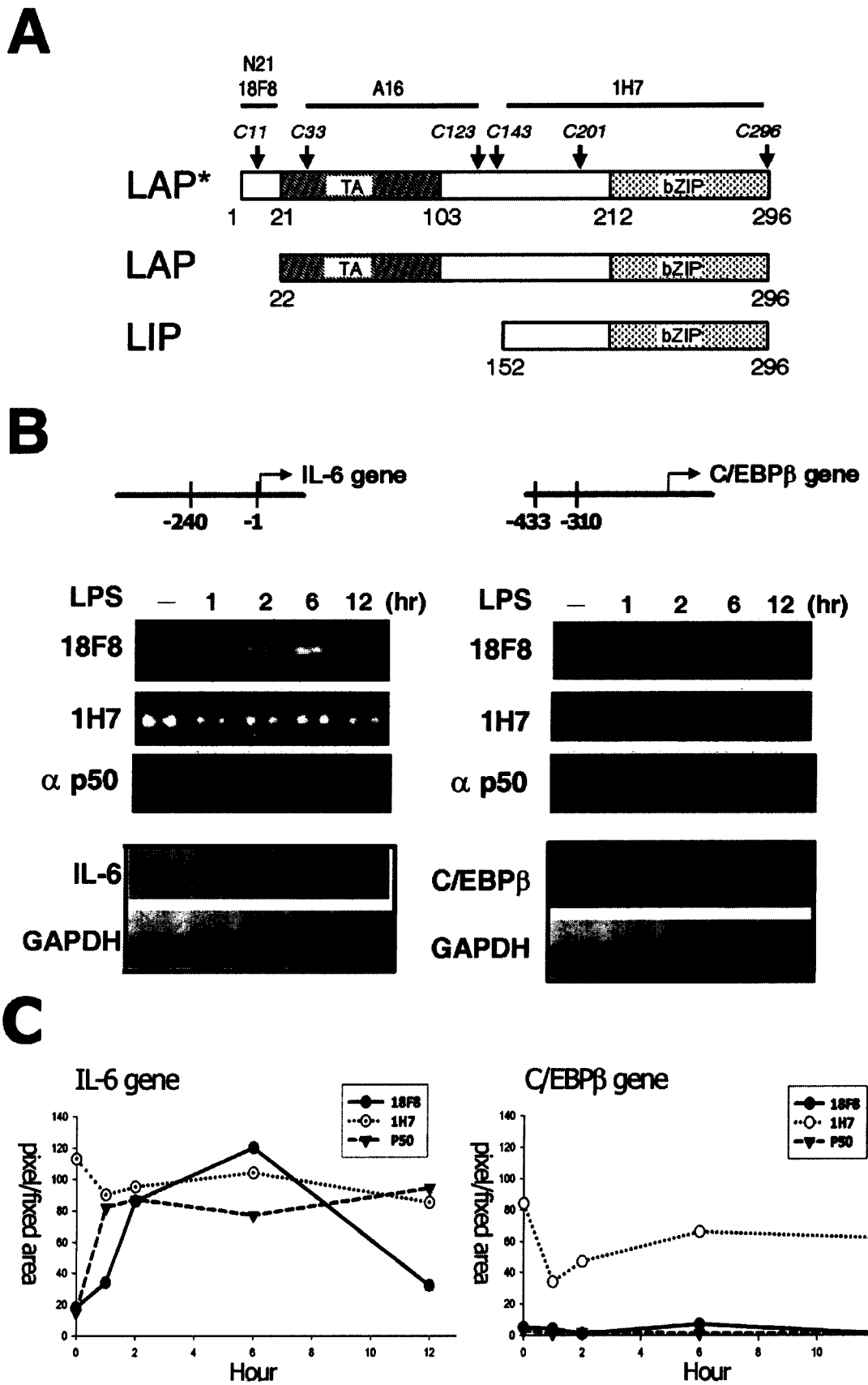

FIG. 1. **LAP* is specifically recruited to IL-6 promoter upon LPS stimulation.** *A*, schematic representation of the C/EBPβ isoforms. The associated *bars* indicate the antigen used to produce the three monoclonal antibodies (18F8, A16, and 1H7) and polyclonal antibody N21. *Arrows*

in LIP (*i.e.* Cys^{201} and Cys^{296}). Monoclonal and polyclonal antibodies that recognize only LAP* (*i.e.* 18F8 and N21), both LAP* and LAP (*i.e.* A16), as well as all three isoforms (*i.e.* 1H7) were generated (Fig. 1*A*, the regions recognized by these monoclonal antibodies are indicated at the *top* of this figure). To investigate the differential recruitment of C/EBPβ isoforms to target gene promoters, 18F8 and 1H7 were employed for chromatin immunoprecipitation (ChIP) experiments of IL-6 and C/EBPβ genes from LPS-treated P388D1(IL1) cells. Schematic representations of these target genes are shown in the *top panels* of Fig. 1*B*. Semi-quantitative analysis of the amounts of DNA immunoprecipitated by 18F8, 1H7, and anti-p50 antibody is shown in Fig. 1*C*. LAP* is selectively recruited to the IL-6 gene promoter only after LPS stimulation, whereas the binding of the sum of all three C/EBPβ isoforms as visualized by ChIP using 1H7 remains constant, independent of the time course of LPS treatment (Fig. 1*B*, *18F8* and *1H7* of *left panels*). The binding of LAP* to the promoter region of C/EBPβ is undetectable as demonstrated by ChIP assay with 18F8, but the time course of 1H7 binding to the C/EBPβ promoter remains unchanged upon LPS treatment (Fig. 1*B*, *18F8* and *1H7* of *right panels*).

NF-κB, known as the predominant factor responsible for the induction of inflammatory cytokine genes (41), was also tested in ChIP experiment with anti-p50 antibody. Indeed, NF-κB was also recruited to the IL-6 promoter, albeit with different kinetic pattern from that of LAP* (Fig. 1*B*, *α p50* of *left panels*). The kinetics of LAP* recruitment to the IL-6 promoter correlates well with the expression of IL-6 mRNA (Fig. 1*B*, *18F8* and *IL-6* of *left panels*). C/EBPβ is constitutively expressed in P388D1(IL1) cells (Fig. 1*B*, *C/EBPβ* of *right panels* and data not shown). Neither LAP* nor NF-κB was recruited to the C/EBPβ promoter upon LPS treatment of P388D1(IL1) cells (Fig. 1*B*, *18F8* and *α p50* of *right panels*). Taken together, these results suggest that LAP* may play key roles for LPS-induced IL-6 expression but not in the constitutive expression of C/EBPβ gene. In addition to, or in conjunction with LAP*, NF-κB could also play important roles in LPS-mediated IL-6 gene expression.

LAP Activation Correlates with the Reduction of Intramolecular Disulfide Bonds*—We next aimed to examine the potential mechanisms that govern the LPS-induced recruitment of LAP* to the IL-6 gene promoter. A number of different pathways have been described to activate C/EBPβ, including transcriptional up-regulation, post-translational modifications, and nuclear translocation (42). The Northern data in Fig. 1*B* (*C/EBPβ panel*) exclude the possibility of transcriptional up-regulation in the present assay system. Immunological analyses demonstrated that both protein level and subcellular localization of C/EBPβ isoforms remain unchanged regardless of whether the P388D1(IL1) cells were treated with LPS or not (data not shown). Because LPS treatment is associated with alterations of the redox state, we hypothesized that LAP* could be regulated by a redox switch. Interestingly, amino acid alignment shows that the cysteine residues in C/EBPβ are highly conserved among species (Fig. 2*A*). Moreover, an extra cysteine residue is located in the N-terminal 21-amino acid stretch that is unique to LAP* (Fig. 2*A*). To assess whether these cysteine residues were involved in disulfide bond rearrangements during LPS treatment, we performed Western blot analysis to LPS-treated P388D1(IL1) under nonreducing conditions. Iodoacetamide was used to trap the free thiol groups during LPS treatment. At least two species of LAP* displaying slower mobility were observed 1 h after LPS treatment (Fig. 2*B*), suggesting the differential reduction of intramolecular disulfide bonds. The kinetics of these mobility changes in LAP* also correlates with the ChIP pattern of 18F8 antibody and the induction of IL-6 gene depicted in Fig. 1*B*. However, when the same protein preparations were subjected to a treatment with the reducing agent DTT, no mobility change could be observed (Fig. 2*B*, *upper panel*). On the contrary, LAP does not show a similar change of mobility under nonreducing conditions (Fig. 2*B*, *bottom panel*). These observations suggest that endogenous LAP* exists in a more compact conformation, which is relaxed by disulfide bond reduction upon LPS stimulation. To further confirm this finding, we treated the nuclear extract of P388D1(IL1) cells with various concentrations of DTT and analyzed by Western blot under nonreducing conditions. As shown in Fig. 2*C*, the N21 antibody detected three different migration forms of LAP* (*upper panel*). A slightly slower migration form was also observed for LAP from the same extracts (Fig. 2*C*, *lower panel*), whereas no mobility change was detected in LIP (data not shown). The same migration behavior was also observed for FLAG-tagged recombinant C/EBPβs expressed in 293T cells (Fig. 2*D*).

Identification of the Intramolecular Disulfide Bonds in LAP and LAP*—To determine which cysteine residues are involved in the intramolecular disulfide bond formation in LAP* and LAP, we performed mass spectrometric analysis. FLAG-LAP* was digested with trypsin, and the resulting peptides were analyzed by mass spectrometer. Disulfide bonds between Cys^{11} and Cys^{33}, between Cys^{123} and Cys^{143}, and between Cys^{201} and Cys^{296} of LAP* were identified (Fig. 3*A*). When FLAG-LAP was subjected to a similar analysis, only Cys^{123} and Cys^{201} were found to form intramolecular disulfide bond. This result is consistent with the barely detectable mobility shift of endogenous LAP shown in Fig. 2*B*. The major determinant in disulfide bond formation between LAP* and LAP hinges on the Cys^{11} residue of LAP*. To assess the importance of this residue in the overall disulfide bond formation, we performed site-directed mutagenesis that substituted the cysteine with a serine residue. Analysis of this mutant FLAG-LAP* (C11S) reveals that only Cys^{123} and Cys^{201}, and not Cys^{11} and Cys^{33} nor Cys^{201} and Cys^{296}, were linked by disulfide bond formation. When Cys^{11} is substituted, the tertiary structure of FLAG-LAP*(C11S) is apparently similar to that of LAP. To correlate these results, we expressed each mutant of the cysteine residues of LAP* and examined their migration pattern under nonreducing SDS-PAGE. As shown in Fig. 3*B*, all of the mutants migrate more slowly than the wild type protein. The mobility of C123S, C143S, C201S, and C296S was somewhat diffused as compared with that of C11S and C33S. The mobility of C11S and C33S was similar, in accordance to their partnership in disulfide bond formation. Taken together, these data provide evidence that all of the cysteine residues in LAP* are linked by disulfide bond formation. Cys^{11} plays a central role in determining the tertiary structure of LAP*. If the disulfide bond between Cys^{11} and Cys^{33} is disrupted by point mutation, LAP* assumes a conformation that is similar to that of LAP.

Transcriptional Activity of LAP Is Greatly Enhanced under*

mark the six highly conserved cysteine residues. *TA*, transactivation domain; *bZIP*, basic leucine zipper domain. *B*, the kinetics of promoter binding and the expression profiles of C/EBPβ target genes. Transcription initiation site on IL-6 and C/EBPβ gene promoters (*arrows*) and the PCR fragments amplified (*line drawings*) are indicated. ChIP experiments were performed with 18F8, 1H7, and anti-NFκB p50 antibodies from P388D1(IL1) cells at the indicated times after LPS stimulation (1 μg/ml). Steady-state RNA levels are monitored by Northern blotting, GAPDH serves as a loading control (*boxed panels*). *C*, semi-quantitative analysis of the ChIP results are represented as the mean intensity over the fixed area normalized against background values.

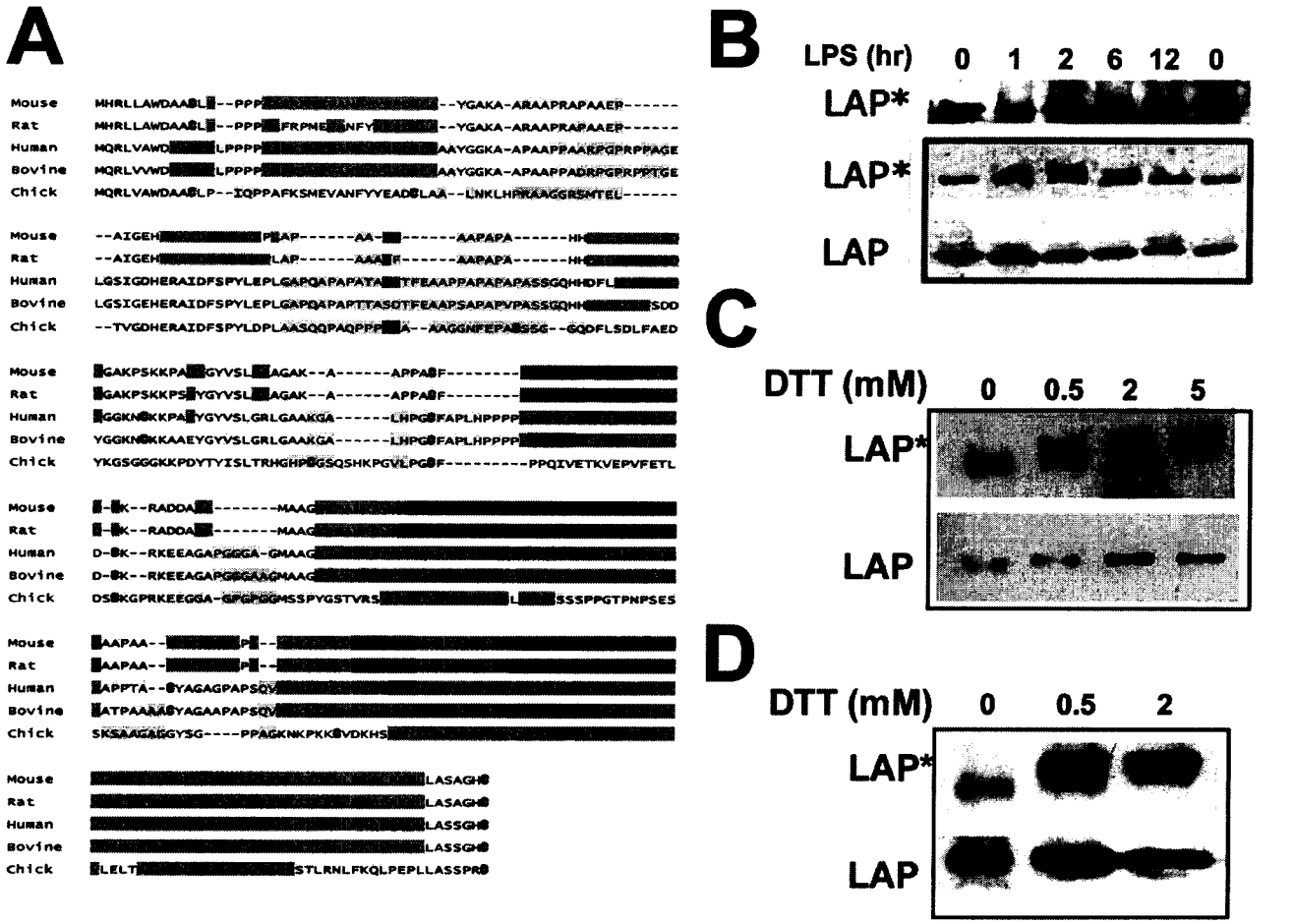

FIG. 2. **LPS induces reduction of disulfide bonds in LAP*.** *A*, amino acid sequence alignment of C/EBPβ from various species. The conserved cysteines are shown in *bold type*. *B*, LAP* displays redox-sensitive mobility changes during LPS stimulation. P388D1(IL1) cells were treated with 1 μg/ml LPS in the presence of 0.1 mM iodoacetamide. The cell lysates harvested at the indicated time were subjected to reducing and nonreducing (*boxed panels*) SDS-PAGE and visualized by Western blot with the N21 (LAP*) and A16 (LAP) antibodies. *C* and *D*, presence of intramolecular disulfide bonds in endogenous and recombinant LAP*. Nuclear extracts from P388D1(IL1) cells (*C*) and C/EBPβ-transfected 293T cells (*D*) were prepared with buffers devoid of DTT. Nuclear extract was incubated with various concentrations of DTT at 37 °C for 20 min. The reaction mixtures were subjected to nonreducing SDS-PAGE and visualized as in *B*.

Reducing Conditions—Having demonstrated that LAP* undergoes reduction of disulfide linkages and activation upon LPS stimulation, we then evaluated the effect of reducing power on the transcription activity of LAP*. The expression vectors of LAP* and LAP were transfected into 293T cells together with AGP-CAT reporter. Consistent with our previous results published elsewhere, LAP is more active than LAP* when tested by transient transfection experiments (15). When LAP* transfectants were treated with the reducing agents PDTC or NAC, the activation of reporter gene was enhanced in a PDTC and NAC concentration-dependent manner. These stimulatory effects were not observed for LAP transfectants (Fig. 4, *A*, *PDTC*, and *B*, *NAC*). These reducing agents may exert their effect by directly reducing the disulfide bonds in LAP*. To explore this possibility, we assayed the transcription activity of the cysteine mutants, which mimic the reduction of their respective disulfide bonds. For C11S and C33S, the transactivation of AGP-CAT was greatly enhanced as compared with that of wild type LAP* and other cysteine mutants (Fig. 4*C*). Because the results shown in Fig. 3 implicate that the C11S mutant (and possibly C33S as well) adopt the same disulfide linkage as in LAP, the most reasonable explanation for these observations is that PDTC or NAC also promotes the disengagement of disulfide linkage between Cys^{11} and Cys^{33}, rendering LAP* to acquire the disulfide pairing as in LAP, which is the most transcriptionally active isoform.

*Reducing Conditions Enhance the DNA Binding Activity of LAP**—To determine the mechanism by which change in redox state influences the transcription activity of LAP*, we performed electrophoretic mobility shift assays. The DNA binding activity of FLAG-LAP*, but not FLAG-LAP and FLAG-LIP, was enhanced by the addition of DTT (Fig. 5*A*, compare *lanes 3* and *6* for LAP*, *lanes 4* and *7* for LAP, and *lanes 5* and *8* for LIP). Similarly, the DNA binding activity of endogenous LAP* was detected only in the DTT-treated extracts, as demonstrated by the antibody-specific supershifts (Fig. 5*B*, compare *lanes 3*, *4*, *9*, and *10*; *asterisks* mark the supershifted complexes). The DNA binding activity of LAP did not appear to be influenced by the presence of DTT (Fig. 5*B*, compare *lanes 5*, *6*, *11*, and *12*; supershifted complex detected by A16). One could argue that DTT may not reflect *in vivo* conditions. To explore the impact of endogenous redox-sensing systems on LAP*, we tested the effects of NADPH, thioredoxin, and the combination of NADPH, thioredoxin, and thioredoxin reductase in electrophoretic mobility shift assays. FLAG-LAP* was purified with M2 beads to avoid the consumption of reducing agents from other proteins. As shown in Fig. 5*C*, DTT (*lanes 2* and *3*) and thioredoxin (*lanes 6* and *7*) were effective in enhancing the

balt3/bc-bc/bc-bc/bc0104/bc9124-04g stafford S=3 5/11/03 4:39 Comments: ARTNO: M305501200

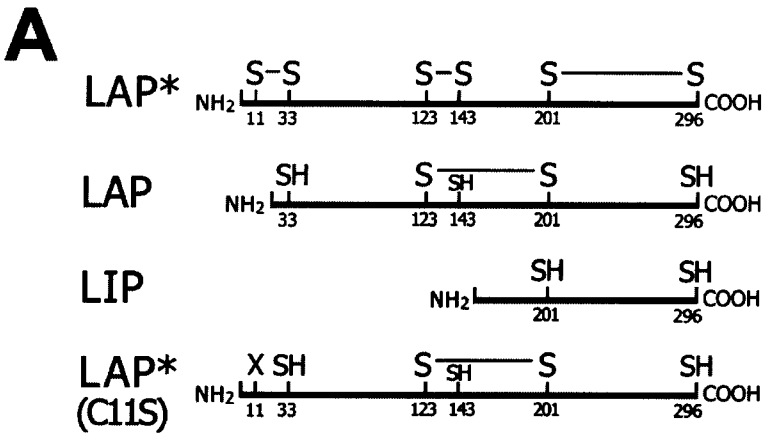

FIG. 3. **Mapping of intramolecular disulfide bond(s) in C/EBPβ.** *A*, schematic representation of the identified intramolecular disulfide bonds of C/EBPβ isoforms. FLAG-tagged C/EBPβs were expressed in 293T cells, immunoaffinity-purified with M2 beads, and recovered from SDS-PAGE. The peptides generated by trypsin digestion were analyzed with LCQ (Finnigan) and MALDI-TOF. *B*, wild type (*WT*) and mutant LAP*s migrate differently in nonreducing SDS-PAGE. FLAG-LAP* and its cysteine mutants (Cys → Ser) were expressed in 293T cells. Nuclear extract prepared with buffer devoid of DTT was subjected to SDS-PAGE and visualized by Western blot with M2 antibody.

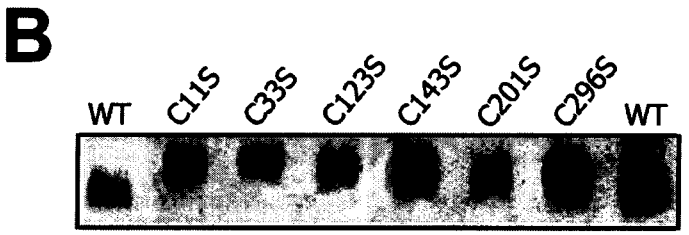

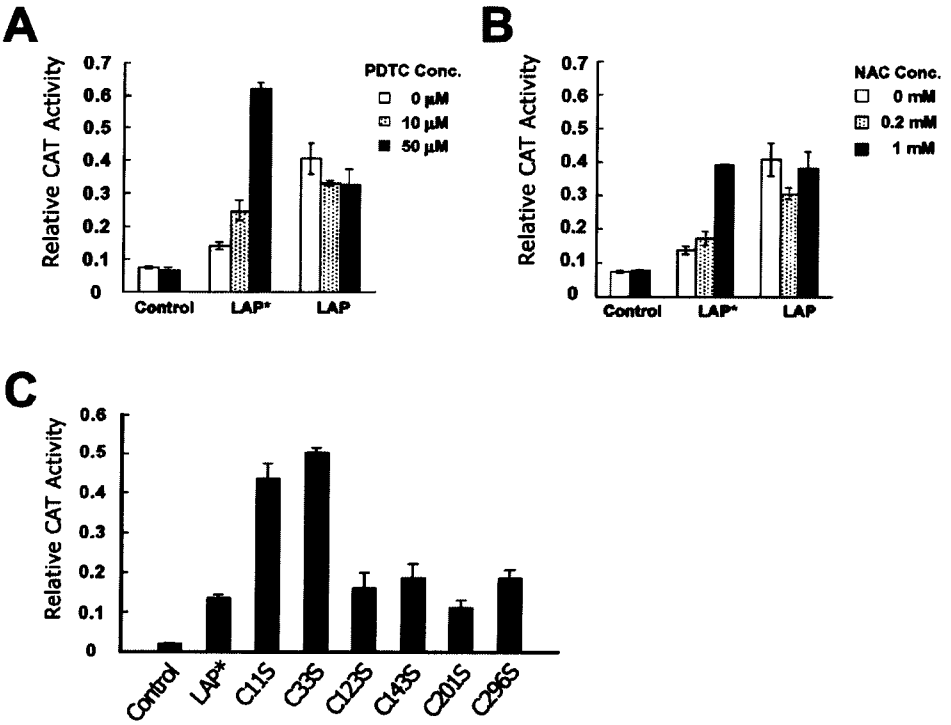

FIG. 4. **The transcriptional activity of LAP*, but not LAP, is enhanced under reducing conditions.** *A* and *B*, treatment with antioxidants stimulates the transactivity of LAP*. 293 T cells were transfected with 1 μg of AGP-CAT, 0.5 μg of pSV-β-galactosidase, and 50 ng of pCMV-tag-LAP* or pCMV-tag-LAP. The transfected cells were treated with various concentrations of PDTC (*A*) and NAC (*B*) for 16 h before harvesting for CAT assays. The CAT activity was normalized with β-galactosidase. *C*, transcriptional activity of LAP* and each cysteine mutants were measured by CAT assay. 293T cells were co-transfected with 0.75 μg of AGP-CAT, 0.25 μg of pSV-β-galactosidase, and 0.02 μg of each corresponding LAP* construct. The CAT assays were performed 36 h post-transfection. Each normalized CAT value represents the means of four independent experiments.

DNA binding activity of LAP*. The reducing effect of thioredoxin alone seemed less effective than that of DTT or the combination of thioredoxin, thioredoxin reductase, and NADPH. This may be attributed to the decreased reducing power by partially oxidized form of thioredoxin. NADPH has an almost undetectable effect (Fig. 5*C*, *lanes 4* and *5*). When LAP* was treated with thioredoxin, NADPH, and thioredoxin reductase, its DNA binding activity was comparable with that of DTT-treated samples (Fig 5*C*, *lanes 8* and *9*). Taken together, our findings provide strong evidence that the DNA binding

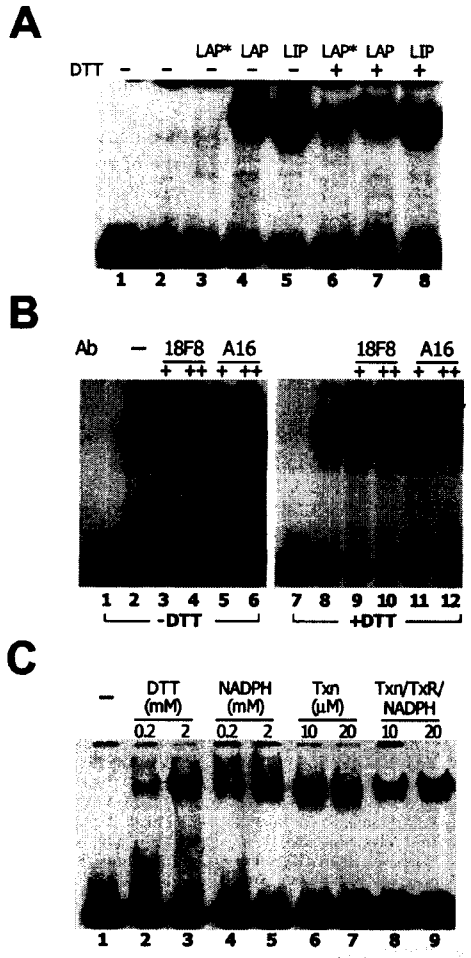

FIG. 5. **The DNA binding activity of LAP* is enhanced under reducing conditions.** *A*, nuclear extracts (5 μg) from 293T cells expressing various recombinant C/EBPβ isoforms were incubated in the absence (*lanes 1–5*) or presence (*lanes 6–8*) of DTT, reacted with [α-^{32}P]ATP-labeled probe, and then separated by 5% native PAGE. *Lane 1*, probe only; *lane 2*, nuclear extract from mock transfected 293T cells; *lanes 3* and *6*, LAP*; *lanes 4* and *7*, LAP; *lanes 5* and *8*, LIP. *B*, 10 μg of nuclear extract from P388D1(IL1) cells were treated in the absence or presence of DTT. The reaction mixtures were then incubated with labeled probe in the absence or presence of antibodies specific to C/EBPβ isoforms. The *asterisks* indicate the supershifted complexes. Two different dosages of antibodies were used: 1 μl (+) and 2 μl (++). *C*, recombinant FLAG-LAP* was purified from 293T transfected cells by immunoprecipitation and eluted with FLAG peptide. The purified FLAG-LAP* was incubated with various reducing agents and further reacted with probe. *Lane 1*, FLAG-LAP* only; *lanes 2* and *3*, 0.2 and 2 mM of DTT; *lanes 4* and *5*, 0.2 and 2 mM NADPH; *lanes 6* and *7*, 10 and 20 μM thioredoxin (*Txn*); *lanes 8* and *9*, thioredoxin reductase (*TxR*) and NADPH and 10 and 20 μM Txn were added to the reaction mixtures.

activity of LAP* may be regulated in a redox-sensitive manner. The thioredoxin and thioredoxin reductase are among the candidate players in the activation of LAP*. In contrast, LAP and LIP are insensitive to the change in redox condition.

DISCUSSION

C/EBPβ is one of the key players in the regulation of growth, differentiation, metabolism, and inflammation. Understanding the mechanism of differential regulation of C/EBPβ is an important issue for basic and applied biological research. Although functional differences have been described between LAP* and LAP (15, 16), how they are separately regulated remains completely unknown. In the present study, we report for the first time that upon LPS stimulation, the full-length isoform LAP* is differentially activated by a redox switch mechanism, and consequently, LAP* gains DNA binding activity and is recruited to the IL-6 promoter for its transcriptional induction.

Because numerous studies revealed that C/EBPβ regulation is extremely complicated and cell type-specific (42), we focused our studies in the P388D1(L1) cells, in which both inducible (IL-6) as well as constitutive regulation (C/EBPβ itself) by C/EBPβ are well documented. The observation that although a bulk of C/EBPβ is permanently associated with both target promoters, the induction of IL-6 does not occur until the recruitment of LAP* strongly suggests that LAP* is the determinant isoform in LPS-inducible IL-6 expression. On the other hand, LAP* does not seem to be involved in the regulation of constitutively expressed genes, as exemplified by C/EBPβ itself. This is in pretty good agreement with our previous report that LAP* preferentially interacts with NF-κB in a synergistic manner, whereas LAP does not. NF-κB is known to be a crucial factor in the LPS-inducible expression of inflammatory cytokine genes (41). Our ChIP data confirmed its initial recruitment to the IL-6 promoter simultaneously with LAP*; nevertheless, NF-κB binding persisted long after decreased IL-6 mRNA production. This difference in promoter binding kinetics prompted us to examine another LPS-inducible gene, TNF-α, for which NF-κB is considered as the determinant factor of its expression. We found that both C/EBPβ and NF-κB were recruited to the TNF-α promoter with the same kinetics (data not shown). A possible implication of these results is that although the activation of C/EBPβ and NF-κB are both necessary for the induction of LPS-up-regulated genes, they may differ in playing the triggering roles for specific genes. In light of the perfect correlation between IL-6 transcription and LAP* recruitment to its promoter, our data strongly suggest that LAP* may play the switch roles for IL-6 transcription, whereas NF-κB plays the key role for the induction of TNF-α gene.

A previous report described the association of LAP* with the SWI-SNF complex through the 21-amino acid stretch in the N terminus (16). It is then speculated that LAP* may be involved in the activation of those target genes requiring chromatin remodeling activity provided by the SWI-SNF complex. The roles of LAP* on chromatin remodeling of the IL-6 and C/EBPβ genes would be crucial for further investigation. Moreover, our biochemical studies demonstrated a novel function for the extra amino acids at the N terminus of LAP*. Specifically, Cys^{11} is clearly involved or affected in the intramolecular disulfide bond formation of LAP*. When cDNA of C/EBPβ is transfected into cells, proteins of all three isoforms are produced. To obtain any single species of C/EBPβ isoform, FLAG-tagged cDNA is used for generating recombinant protein by transient transfection into host cells. When we performed SDS-PAGE and Western blot analysis under nonreducing and reducing conditions using P388D1(IL1)-derived and FLAG-tagged proteins, the mobility of endogenous-derived and recombinant proteins are similar. This result suggests that the intramolecular disulfide bond formation for endogenous and recombinant proteins is likely to be the same. Mass spectra analysis indicates that Cys^{11} and Cys^{33}, Cys^{123} and Cys^{143}, and Cys^{201} and Cys^{296} of LAP* form three intramolecular disulfide bonds. LAP, lacking the N-terminal 21 amino acids and thus Cys^{11}, is different from LAP* in tertiary structure. The intramolecular disulfide bond of LAP is between Cys^{123} and Cys^{201}. The intramolecular disulfide bond of LAP*(C11S) is the same as that of LAP. These results indicate that Cys^{11} of LAP* is key to the tertiary structure of LAP*. The Cys^{11} and Cys^{33} disulfide bond could affect the function of the transactivation domain of LAP*. Maybe when Cys^{11} gets reduced under redox switch, the conformation of LAP* changes to facilitate its association with the SWI-SNF complex and

hence turning on target gene expression (16). Therefore, the activities of LAP* and LAP are likely to be different, and LAP* may be the primary factor among C/EBPβ isoforms that confers the redox-sensitive transactivation of target genes.

Closely related family member proteins were known to display different activities because of the difference in their intramolecular disulfide bonds (43). For example, insulin-like growth factor (IGF)-binding proteins (IGFBPs 1–6) are responsible for modulating the action of IGFs. IGFBPs 1–5 contain 18 conserved cysteines, but IGFBP-6 lacks two of the 12 N-terminal cysteines. The N-terminal intramolecular disulfide linkages of IGFBP-6 differ significantly from those of IGFBP-1 as determined by mass spectrometry. This difference could contribute to the distinctive IGF binding properties of IGFBP-6 (which has the highest affinity for IGF-II). Our present results on the difference of intramolecular disulfide bonds between LAP* and LAP are analogous to those of IGFBPs.

How does LAP* get reduced in LPS-treated P388D1(IL1) cells? The more likely physiological scenario is through oxidoreductases (*e.g.* thioredoxin and thioredoxin reductase). There is a report on the elevation of thioredoxin and thioredoxin reductase levels in placenta of pregnant mice exposed to LPS (18). The LPS-treated P388D1(IL1) cells may generate high levels of thioredoxin, thioredoxin reductase, and NADPH and thus facilitate the activation of LAP*. Alternatively, oxidoreductase such as protein disulfide isomerase may be activated under LPS-stimulated conditions and may then activate LAP*. Our results demonstrated that LAP* gets reduced when P388D1(IL1) cells are treated with LPS (Fig. 2*B*). These results suggest that post-translational events, such as the reduction of disulfide bonds are responsible for the activation of LAP*. Consistent with the ChIP results, transient transfection experiments using wild type LAP* also demonstrated that LAP*, not LAP, is specifically activated by PDTC or NAC treatment. When treated with 50 μM PDTC, the transcription activity of LAP* is higher than that of LAP. The transactivation activity of LAP*(C11S) or LAP*(C33S) is much higher than that of wild type LAP*, suggesting that the reduction of intramolecular disulfide bond between Cys^{11} and Cys^{33} of LAP* may be important for its activation. The intramolecular disulfide bond between Cys^{201} and Cys^{296} may pose a constraint for dimerization of LAP*, which must be reduced or disrupted preceding DNA binding. Alternatively, Cys^{11} or Cys^{33} may influence the overall tertiary structure and conformation during protein translation. That is why when Cys^{11} is mutated, the intramolecular disulfide bond of LAP*(C11S) is the same as LAP. The disulfide bond between Cys^{123} and Cys^{201} may be buried in the molecule based on the results of our molecular modeling (data not shown). The DNA binding activity of LAP* is activated by reducing agents, whereas LAP is constitutively active. In addition to playing roles of direct disulfide bond formation, Cys^{11} could influence the folding of LAP* during translation. Mutation of cysteine residues other than Cys^{11} and Cys^{33} could have very different effects on intramolecular disulfide bond formation and folding of LAP*. The results from transient transfection experiments performed with various cysteine mutants clearly define that Cys^{11} and Cys^{33} are functionally different from other cysteines (Fig. 5*C*). In addition to dimerization and DNA binding, domain(s) located near the N-terminal region is important for the transactivation of LAP*. Cys^{11} and Cys^{33} could influence the disulfide bonds formation mediated by the other four cysteines; however, the other mutants of cysteines (*i.e.* Cys^{123}, Cys^{143}, Cys^{201}, and Cys^{296}) may or may not influence the disulfide bond formation between Cys^{11} and Cys^{33}. These possibilities are to be addressed in future experiments. Any results derived from the mutation of cysteine must be interpreted with caution. It should also be noted that, because resident genes are embedded in chromatin but the ectopically transfected plasmids are not, the activities of LAP* defined by transient transfection and those derived from the ChIP for are likely to be different.

The results from this study suggest that LAP* may function as a cellular sensor for the sudden surge of reducing potential that is required for switching the key regulatory genes as exemplified by the induction of IL-6 gene. LAP, on the other hand, does not respond to the reducing power but may regulate the transcription of genes with house keeping functions. Taken together, these results demonstrate that redox switch is responsible for the activation of LAP*, but not LAP, for targeting genes encoding key regulatory proteins. This novel type of molecular switch for differential regulation of two transcriptional activators resulted from alternative translation of the same mRNA, may be found in other systems, and should have general interest in studying gene regulation.

Acknowledgments—We thank Li-Ping Tu, Ruey Chao, and Han Ting Chou for excellent technical assistance.

REFERENCES

1. Lekstrom-Himes, J., and Xanthopoulos, K. G. (1998) *J. Biol. Chem.* **273,** 28545–28548
2. Poli, V. (1998) *J. Biol. Chem.* **273,** 29279–29282
3. Akira, S., Isshiki, H., Sugita, T., Tanabe, O., Kinoshita, S., Nishio, Y., Nakajima, T., Hirano, T., and Kishimoto, T. (1990) *EMBO J.* **9,** 1897–1906
4. Chang, C. J., Chen, T. T., Lei, H. Y., Chen, D. S., and Lee, S. C. (1990) *Mol. Cell. Biol.* **10,** 6642–6653
5. Pope, R. M., Leutz, A., and Ness, S. A. (1994) *J. Clin. Invest.* **94,** 1449–1455
6. Zhang, Y., and Rom, W. N. (1993) *Mol. Cell. Biol.* **13,** 3831–3837
7. Shirakawa, F., Saito, K., Bonagura, C. A., Galson, D. L., Fenton, M. J., Webb, A. C., and Auron, P. E. (1993) *Mol. Cell. Biol.* **13,** 1332–1344
8. Bretz, J. D., Williams, S. C., Baer, M., Johnson, P. F., and Schwartz, R. C. (1994) *Proc. Natl. Acad. Sci. U. S. A.* **91,** 7306–7310
9. Hu, H. M., Tian, Q., Baer, M., Spooner, C. J., Williams, S. C., Johnson, P. F., and Schwartz, R. C. (2000) *J. Biol. Chem.* **275,** 16373–16381
10. Pope, R., Mungre, S., Liu, H., and Thimmapaya, B. (2000) *Cytokine* **12,** 1171–1181
11. Williams, S. C., Baer, M., Dillner, A. J., and Johnson, P. F. (1995) *EMBO J.* **14,** 3170–3183
12. Descombes, P., and Schibler, U. (1991) *Cell* **67,** 569–579
13. Diehl, A. M., Michaelson, P., and Yang, S. Q. (1994) *Gastroenterology* **106,** 1629–1637
14. Raught, B., Liao, W. S., and Rosen, J. M. (1995) *Mol. Endocrinol.* **9,** 1223–1232
15. Lee, Y. M., Miau, L. H., Chang, C. J., and Lee, S. C. (1996) *Mol. Cell. Biol.* **16,** 4257–4263
16. Kerppola-Leutz, E., and Leutz, A. (1999) *Mol. Cell* **4,** 735–743
17. Matsusaka, T., Fujikawa, K., Nishio, Y., Mukaida, N., Matsushima, K., Kishimoto, T., and Akira, S. (1993) *Proc. Natl. Acad. Sci. U. S. A.* **90,** 10193–10197
18. Kojima, K., Koji, T., Nanri, H., Kashimura, M., and Ikeda, M. (1999) *Placenta* **20,** 561–566
19. Rosenspire, A. J., Kindzelskii, A. L., and Petty, H. R. (2002) *J. Immunol.* **169,** 5396–5400
20. Bochkov, V. N., Kadl, A., Huber, J., Gruber, F., Binder, B. R., and Leitinger, N. (2002) *Nature* **419,** 77–81
21. Bauer, C. E., Elsen, S., and Bird, T. H. (1999) *Annu. Rev. Microbiol.* **53,** 495–523
22. Pomposiello, P. J., and Demple, B. (2001) *Trends Biotechnol.* **19,** 109–114
23. Carmel-Harel, O., and Storz, G. (2000) *Annu. Rev. Microbiol.* **54,** 439–461
24. Zheng, M., and Storz, G. (2000) *Biochem. Pharmacol.* **59,** 1–6
25. Abate, C., Patel, L., Rauscher, F. J., III, and Curran, T. (1990) *Science* **249,** 1157–1161
26. Pognonec, P., Kato, H., and Roeder, R. G. (1992) *J. Biol. Chem.* **267,** 24563–24567
27. Hayashi, T., Ueno, Y., and Okamoto T. (1993) *J. Biol. Chem.* **268,** 11380–11388
28. Markus, M., and Benezra, R. (1999) *J. Biol. Chem.* **274,** 1040–1049
29. Nakshatri, H., Bhat-Nakshatri, P., and Currie, R. A. (1996) *J. Biol. Chem.* **271,** 28784–28791
30. Grant, C. M. (2001) *Mol. Microbiol.* **39,** 533–541
31. Toone, W. M., Morgan, B. A., and Jones, N. (2001) *Oncogene* **20,** 2336–2346
32. Xanthoudakis, S., and Curran, T. (1992) *EMBO J.* **11,** 653–665
33. Myrset, A. H., Bostad, A., Jamin, N., Lirsac, P. N., Toma, F., and Gabrielsen, O. S. (1993) *EMBO J.* **12,** 4625–4633
34. Storz, G., Tartaglia, L. A., Farr, S. B., and Ames, B. N. (1990) *Trends Genet.* **6,** 363–368
35. Guehmann, S., Vorbrueggen, G., Kalkbrenner, F., and Moelling, K. (1992) *Nucleic Acids Res.* **20,** 2279–2286
36. Matthews, J. R., Wakasugi, N., Virelizier, J. L., Yodoi, J., and Hay, R. T. (1992)

JOBNAME: AUTHOR QUERIES PAGE: 1 SESS: 1 OUTPUT: Tue Nov 4 07:29:12 2003
/balt3/bc-bc/bc-bc/bc0104/bc9124-04g

AUTHOR QUERIES

AUTHOR PLEASE ANSWER ALL QUERIES 1

A—Au: Please provide the postal code(s) for the affiliation line.

B—Au: Please write out the definition for "C/EBP" in "a member of the C/EBP family" in the summary and add it to the abbreviation footnote.

C—Au: The Journal guidelines state that the summary should fit into the left-hand column. If your summary is long enough to run over into the right-hand column, please cut text.

D—Au: Again, please add the definition for C/EBP to the abbreviation footnote.

E—Au: G-CSF was used only once, and most abbreviations must be used at least five times in the text to be allowed according to Journal style. Please verify definition.

F—Au: If SWI-SNF is an abbreviation, please add the definition to the abbreviation footnote.

G—Au: Please write out the definition for LC ESI in the heading.

H—Au: If LCQ is an abbreviation, please write out the definition. It is used only twice.

I—Au: If you do not want your fax and phone numbers and e-mail address printed, please delete them.

J—Au: Please verify the definition(s) in the abbreviation footnote.

Nucleic Acids Res. **20,** 3821–3830
37. McBride, A. A., Klausner, R. D., and Howley, P. M. (1992) *Proc. Natl. Acad. Sci. U. S. A.* **89,** 7531–7535
38. Lee, Y. M., Tsai, W. H., Lai, M. Y., Chen, D. S., and Lee, S. C. (1993) *Mol. Cell. Biol.* **13,** 432–442
39. Duong, D. T., Waltner-Laws, M. E., Sears, R., Sealy, L., and Granner, D. K. (2002) *J. Biol. Chem.* **277,** 32234–32242
40. Mancini, R., Fagioli, C., Fra, A. M., Maggioni, C., and Sitia, R. (2000) *FASEB J.* **14,** 769–778
41. Sweet, M. J., and Hume, D. A. (1996) *J. Leukocyte Biol.* **60,** 8–26
42. Bradley, M. N., Zhou, L., and Smale, S. T. (2003) *Mol. Cell. Biol.* **23,** 4841–4858
43. Neumann, G. M., and Bach, L. A. (1999) *J. Biol. Chem.* **274,** 14587–14594